

On Charting Global Ocean Tides

ERNST W. SCHWIDERSKI

U.S. Naval Surface Weapons Center, Dahlgren, Virginia 22448

This review article highlights the three-century development of our scientific understanding of ocean tides, culminating through myths, paradoxes, and controversies in a global tide model that now permits the prediction of the instantaneous total tide anywhere in the open oceans with an accuracy of better than 10 cm. All major aspects of tidal research, including empirical, mathematical, and empirical-mathematical methods, are considered. Particular attention is drawn to the most recently developed computerized techniques comprehending hydrodynamical dissipation and secondary tide-generating forces, finite-differencing schemes, geometric boundary and bathymetry modeling, and hydrodynamical interpolation of properly selected empirical tide data. Numerous computer experiments are mentioned that were carried out by various researchers in order to evaluate the magnitudes of the featured effects. Further possible improvements are mentioned, especially in nearshore areas, in the Arctic Sea, and near Antarctica, where empirical tide and bathymetry data are either rough or marginal.

CONTENTS

Introduction	243
Elementary approximations.....	244
Harmonic decomposition of equilibrium and ocean tides	244
Empirical methods.....	247
Elementary solutions of Laplace's tidal equations.....	248
Modeling continuous ocean tidal equations.....	249
Continuous ocean tidal equations.....	249
Lateral eddy dissipation	250
Bottom friction laws	252
Secondary tide-generating forces	253
Polar singularities and ice caps	255
Modeling discrete ocean tidal equations.....	255
The gridded ocean basin and bathymetry	255
Discrete ocean tidal equations	256
Lateral empirical and mathematical boundary data.....	258
Discussion of ocean tidal models	260
Evaluation of ocean tidal charts	260
Conclusions	265

1. INTRODUCTION

As is reflected in art, music, and poetry, the restless sea with its surfing waves, swirling currents, and swelling tides has fascinated and frightened mankind from its beginning. All through the ages the mighty erosive and devastating power of ocean tides flooding shorelands and seaports troubled land developers, harbor engineers, and seamen. The observed periodic feature of tides very early led laymen tidalists to record, analyze, and predict high and low tides in coastal waters and to warn and prepare people to take appropriate precautions. Indeed, quite satisfactory tide tables were constructed by simple rules of thumb. Nowadays, in seashore areas, newspapers, radio and television broadcasts, and special bulletins publish daily, monthly, and longer-range tide predictions of interest to many users.

Up to recent years, practical interest in ocean tides was essentially confined to coastal waters. With the advancement of science and technology the need for extremely accurate tide predictions in all the world oceans has become an urgent problem. In fact, ocean tides represent fluctuating loads on the solid earth, which cause tilting of the crust and disturbances of the earth's stress and gravity fields. The precise knowledge of these loads permits researchers to determine important hydrodynamical parameters of the oceans and elastic parameters of the solid earth. Similarly, interactions between

This paper is not subject to U.S. copyright. Published in 1980 by the American Geophysical Union.

ocean tides and atmosphere, celestial bodies, and artificial satellites and missiles can be studied with high accuracy.

Recently, the National Aeronautics and Space Administration and the Department of Defense joined in the common mission to map the geoid at sea by satellite altimetry up to about 10-cm accuracy. However, the geoidal (rest) sea level is hydrodynamically disturbed by ocean tides and other currents due to pelagic density variations and atmospheric surface forces. This review deals only with 'ocean tides' and their corresponding 'tidal currents.' (Other 'general ocean currents or circulations' are mentioned when it is appropriate.) The tidal undulations of the sea surface topography reach amplitudes of more than 100 cm in open oceans and 200 cm in coastal waters. Thus ocean tides (and currents) need to be determined with an accuracy compatible with the desired geoid accuracy in order to provide effective corrections for altimeter measurements.

In brief, contemporary researchers of today in geophysics, geodesy, oceanography, meteorology, astronomy, and space technology all pose the same challenging problem: we need to know, for any given time and place of the world oceans, the tidal elevation of the sea surface over its geoidal level within 10-cm accuracy. It may be emphasized that this modern problem specifies an extraordinary concrete numerical accuracy for its solution. Therefore it is no longer purely an exclusive academic task which is solely concerned with the modeling of general qualitative features of ocean tides.

In the past three centuries, since *Newton* [1687], oceanographers, physicists, and mathematicians devoted an almost unbroken effort to develop realistic models of tides in the global or limited world oceans by (1) empirical methods, that is, by analyzing and extrapolating vast numbers of tidal measurements recorded at continental, island, and deep-sea stations around the world; (2) theoretical methods, that is, by tapping the wealth of analytical and numerical mathematical tools designed for the integration of physically defined hydrodynamical equations governing tidal currents; and (3) hydrodynamical interpolation methods, which combine the purely empirical and theoretical methods 1 and 2 into one consistent technique.

The continuous interest in the theory of ocean tides was enhanced by an international contest conducted by the Paris Academy of Sciences in 1738 [*Cantor*, 1901] with such leading mathematicians as Bernoulli, Euler, and Maclaurin competing for the honor of producing the best tidal model. Yet the un-

derstanding of the captivating phenomena of ocean tides progressed slowly through myths, paradoxes, and heated controversies. Still, in Grenoble an *International Working Group on Ocean Tides* [1975] sponsored by the International Association of the Physical Sciences of the Oceans, the Scientific Committee on Oceanic Research of the International Council of Scientific Unions, and Unesco dissolved itself after a 10-year unsuccessful attempt to map the global ocean tides. The constructed tidal charts predicted low tides for high tides and vice versa over large ocean areas and fell considerably short of the desired numerical accuracy [cf. Cartwright, 1977].

Nevertheless, the qualitative features of the tide models published by, for example, Hansen [1966], Tiron et al. [1967], Pekeris and Accad [1969], Zahel [1970, 1973, 1975], Hendershott [1972], Gordeyev et al. [1973], and Estes [1975] did suggest that significant progress in the understanding of the leading characteristic properties had indeed been made. Subsequently, Estes [1977], Gordeyev et al. [1977], Zahel [1977], Parke and Hendershott [1979], and Accad and Pekeris [1978] improved their earlier models by inclusion of secondary tide-generating forces. Supported by extensive computer experiments, Schwiderski [1976, 1978a, b, 1979a, b, c] improved the dissipative, geometrical, and numerical features of the Hansen-Zahel-Estes method and interpolated hydrodynamically over 2000 empirical tide data. The constructed semidiurnal principal moon (M_2) tide is believed to satisfy the desired accuracy anywhere in the open oceans. In fact, the *International Workshop on Interaction of Marine Geodesy With Inertial, Tidal, and High Frequency Aspects of Ocean Dynamics* [1978] concluded in its final report that techniques are now available to compute the total open ocean tides within the 10-cm accuracy limit.

The following treatise highlights the development of our scientific understanding of ocean tides, culminating in a detailed qualitatively and quantitatively accurate global tidal model. The hydrodynamical-mathematical techniques used in ocean tidal research are, of course, closely related to those developed in the more general field of modeling laminar and turbulent motions of viscous fluids such as ocean currents and atmospheric circulations. The special field of ocean tides, which are distinguished by their simplifying periodic properties and by their widely observed boundary values, may be considered a proving ground for other more involved flow problems.

2. ELEMENTARY APPROXIMATIONS

a. Harmonic Decomposition of Equilibrium and Ocean Tides

Very early scientists linked the periodic feature of ocean tides to the apparent motions of the moon and sun. The first physical explanation of tides was given by Newton [1687], who introduced the still important 'equilibrium theory of tides' as a direct consequence of his newly discovered theory of gravitation. Owing to the inverse square law of mass attraction, the (true) moon (or sun) MT (see Figure 1a) is assumed to attract instantaneously the sea surface point A to A^* and, somewhat less, point B to B^* . At this stage it is commonly concluded that there should be one high tide per day, contrary to the vast majority of observations. However, since the center C of the solid earth is also attracted to about the midpoint C^* between A^* and B^* , one finds, under conservation of mass, Newton's equilibrium tide shown in Figure 1b. It displays high tides on both sides of the earth as if they were generated by two opposing

moons, a true moon MT and a virtual one MV. This simple theory resolved the first tidal paradox that there are two high tides daily, as is observed in most ocean areas. On the other hand, it supported an erroneous myth that high tide should occur directly under the moon.

Strictly, Newton's equilibrium tide provides the tidalist only with the exact astronomical tide-generating potential, to which the ocean responds hydrodynamically in a complex way. The equilibrium theory of tides was perfected in 1738 during the contest of the Paris Academy of Sciences mentioned in section 1. The theoretical and empirical investigations of ocean tides were greatly aided by Lord Kelvin [Thomson, 1868], who, following an earlier suggestion by Laplace, introduced the so-called 'method of harmonic analysis' into tidal research. The astronomical tide-generating potential or equilibrium tide is decomposed into an almost periodic (non-harmonic frequency spectrum) series of harmonic partial tides with each constituent featuring some property of the elliptic and inclined orbits of the moon and earth. Darwin [1883] extended this expansion up to 39 terms, and Doodson [1921] carried it on to 400 frequency modes by introducing his ingenious Doodson numbers. A novel nonharmonic and, subsequently, harmonic decomposition of the equilibrium tide was derived by Cartwright and Tayler [1971].

In directly applicable terms the equilibrium tide (or astronomical tide-generating potential) is decomposed into the series

$$\eta = \sum_{\nu=0} \eta_{\nu}(\lambda, \theta, t) \quad (1)$$

with the following three major species of harmonic partial tides:

Semidiurnal equilibrium tides

$$\nu = 2 \quad \eta = K \sin^2 \theta \cos (\sigma t + \chi + 2\lambda) \quad (2)$$

Diurnal equilibrium tides

$$\nu = 1 \quad \eta = K \sin 2\theta \cos (\sigma t + \chi + \lambda) \quad (3)$$

Long-period equilibrium tides

$$\nu = 0 \quad \eta = K(3 \sin^2 \theta - 2) \cos (\sigma t + \chi) \quad (4)$$

In these equations the following notations are used:

- t universal standard time, seconds;
- λ east longitude;
- θ colatitude;
- η total or partial equilibrium tides, meters;
- $G\eta$ total or partial astronomical tide-generating potential;
- G gravity acceleration, equal to 9.81 m/s^2 ;
- K amplitude of partial equilibrium tide (Table 1), meters;
- σ frequency of partial equilibrium tide (Table 1), s^{-1} ;
- χ astronomical argument of partial equilibrium tide relative to Greenwich midnight (Table 1).

According to the decomposition of the total equilibrium tide (equations (1)-(4)), each harmonic component is completely determined by the three constants (K , σ , χ), listed in Table 1 for the 11 leading modes. As can be verified by other tabulations [e.g., Dietrich, 1963], all other tidal components fall below 4% of the dominating semidiurnal principal moon (M_2) tide and need not be considered in present global ocean tide models. At this point it may be mentioned that the magnitude of the partial equilibrium tide does not necessarily re-

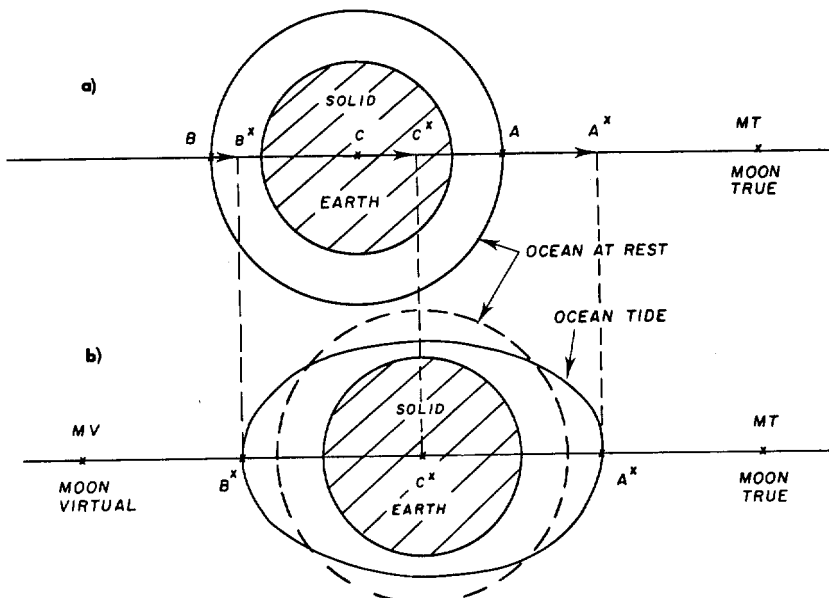


Fig. 1. Newton's equilibrium tide.

fect the magnitude of the corresponding ocean tide. Incidentally, the astronomical argument χ is actually (slightly) time dependent (see Table 1) and requires some updating at least annually.

The harmonic expansion of the tide-generating potential is evidently of fundamental significance for the mathematical analysis and prediction of ocean tides. If one assumes that ocean tides are governed by linear or almost linear equations of motion (equations (18) and (19) or (28) and (29)), then the total oceanic tide is also representable as a linear superposition of harmonic modes. Every harmonic component of the equilibrium tide (equations (2), (3), and (4))

$$(2) \quad \eta = K(\theta) \cos(\sigma t + \chi + \nu\lambda) \quad \nu = 2, 1, 0 \quad (5)$$

generates through the ocean's response a similar oceanic partial tide

$$(3) \quad \xi = \xi(\lambda, \theta) \cos[\sigma t + \chi - \delta(\lambda, \theta)] \quad (6)$$

$$(4) \quad t \rightarrow t - \chi/\sigma \quad (7)$$

TABLE 1. Constants of Major Tidal Modes

Tidal Mode	K, m	$\sigma, 10^{-4}/\text{s}$	χ, deg
<i>Semidiurnal Species. $\nu = 2$</i>			
M_2	principal lunar	0.242334	$2h_0 - 2s_0$
S_2	principal solar	0.112841	0
N_2	elliptical lunar	0.046398	$2h_0 - 3s_0 + p_0$
K_2	declination luni-solar	0.030704	$2h_0$
<i>Diurnal Species. $\nu = 1$</i>			
K_1	declination luni-solar	0.141565	$h_0 + 90$
O_1	principal lunar	0.100514	$h_0 - 2s_0 - 90$
P_1	principal solar	0.046843	$h_0 - 90$
Q_1	elliptical lunar	0.019256	$h_0 - 3s_0 + p_0 - 90$
<i>Long-Period Species. $\nu = 0$</i>			
Mf	fortnightly lunar	0.041742	$2s_0$
Mm	monthly lunar	0.022026	$s_0 - p_0$
Ssa	semiannual solar	0.019446	$2h_0$

K is the amplitude of the partial tide, σ is the frequency of the partial tide, and χ is the astronomical argument of the partial tide. Here h_0 , s_0 , and p_0 are the mean longitudes of the sun and moon and the lunar perigee at Greenwich midnight: $h_0 = 279.69668 + 36,000.768930485T + 3.03 \cdot 10^{-4}T^2$, $s_0 = 270.434358 + 481,267.88314137T - 0.001133T^2 + 1.9 \cdot 10^{-6}T^3$, $p_0 = 334.329653 + 4069.0340329575T - 0.010325T^2 - 1.2 \cdot 10^{-5}T^3$, where $T = (27,392.500528 + 1.0000000356D)/36,525$, $D = d + 365(y - 1975) + \text{Int}[(y - 1975)/4]$, d is the day number of the year ($d = 1$ for January 1), $y \geq 1975$ is the year number, and $\text{Int}[x]$ is the integral part of x .

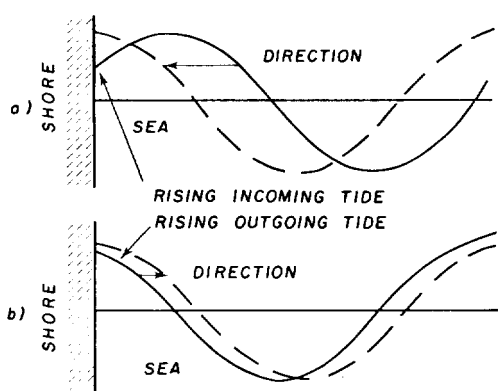


Fig. 2. Rising shore tides. (a) Incoming tidal crest. (b) Outgoing tidal crest.

Of course, when superpositions of partial tides are considered, the universal standard time and the corresponding astronomical arguments must be reintroduced.

In the new individual time count, all long-period equilibrium tides η ((4) and (5); $\chi = 0$) represent standing waves, which at $t = 0$ are at their highs everywhere in the middle latitude zone $|\phi| < 35.26^\circ$ and at their lows in the outside polar zones with the separating nodal line at about $|\phi| = 35.26^\circ$. All diurnal and semidiurnal equilibrium tides η ((2), (3), and (5); $\chi = 0$) represent irreversible strictly westward progressing waves that crest at $t = 0$ at Greenwich (half) meridian $\lambda = 0^\circ$ or full meridian $\lambda = 0^\circ$ and $\lambda = 180^\circ$, respectively. The equator (not meridian) contour of any semidiurnal equilibrium tide is illustrated in Figure 1b.

Without any explicit knowledge of the numerical distribution of the amplitudes and phases (ξ, δ) , one concludes from (6) ($\chi = 0$) that all forced oceanic partial tides ζ represent irreversibly progressing waves that crest at the specified time $t = t_0$ at the 'cotidal line': $\delta(\lambda, \theta) = \sigma t_0$. This simple observation clarifies a widely held myth concerning 'incoming and outgoing tides' at beaches. At shore points, ocean tides are either incoming or outgoing without reversals; that is, the tidal crests always move in from sea to shore (Figure 2a), or the tides swell to their crests first at the shore and then move out to sea (Figure 2b). Of course, the waters always come in from sea, but in a distinctly different fashion for rising incoming and outgoing tides (Figures 2a and 2b). The different curvatures of the rising incoming and rising outgoing tidal waves seem to indicate more stable tidal currents in the latter case. Hence rising incoming tides may display higher and rougher waters

due to bottom disturbances and stresses of winds blowing from sea to shore.

Once the harmonic tidal constants (ξ, δ) are determined for a given geographical location (λ, θ) either by observation and harmonic analysis or by theoretical modeling, then the time-dependent ocean tide ζ can be predicted at any time t by (6). If (ξ_0, δ_0) and (ξ, δ) denote true and empirically or theoretically determined tidal amplitudes and phases, respectively, at any fixed location (λ, θ) , then the time-dependent prediction error is

$$\xi = \xi_0 - \zeta = \xi \cos(\sigma t - \delta) \quad (8)$$

with

$$\xi_0 = \xi_0 \cos(\sigma t_0 - \delta_0) \quad \zeta = \xi \cos(\sigma t - \delta) \quad (9)$$

$$\xi^2 = \xi_0^2 - 2\xi_0 \xi \cos(\delta_0 - \delta) + \xi^2 \quad (10)$$

and

$$\tan \delta = \frac{\xi_0 \sin \delta_0 - \xi \sin \delta}{\xi_0 \cos \delta_0 - \xi \cos \delta} \quad (11)$$

Hence, the 'prediction error E ' is defined by the error amplitude ξ (maximum error) or more appropriately by the standard deviation

$$E = \text{rms}(\xi) = \frac{1}{2} 2^{1/2} \xi \quad (12)$$

Some maximum errors are

$$\xi_M = \xi_M = \xi_0 + \xi \quad \text{for } \delta_0 - \delta = 180^\circ \quad (13)$$

$$\xi_M = \xi_M = \xi_0 - \xi \quad \text{for } \delta_0 - \delta = 0^\circ \quad (14)$$

$$\xi_M = \xi_M = 2\xi \sin \frac{1}{2}(\delta_0 - \delta) \quad \text{for } \xi = \xi_0 \quad (15)$$

and

$$\xi_M = \xi_M = 0.52\xi \quad \text{for } \xi = \xi_0 \quad \text{and } \delta_0 - \delta = 30^\circ \quad (16)$$

$$\xi_M = \xi_M = \xi \quad \text{for } \xi = \xi_0 \quad \text{and } \delta_0 - \delta = 60^\circ \quad (17)$$

From (16) one concludes the important fact that even if a tide model is exact in amplitude ξ , the maximum prediction error is larger than half the tidal amplitude itself for a phase error of 30° (about 1 hour for semidiurnal tides). For a phase error of 60° (equation (17)) the error exactly equals the tide and renders the tidal model completely useless for predictions. This rather severe result displays the extreme complexity needed to achieve the numerical accuracy specified in section

TABLE 2. Bermuda M_2 Tide Observations

Station	Geographic Coordinates		ξ , cm	δ , deg	Reference
	$^{\circ}\text{N}$	$^{\circ}\text{W}$			
St. George's Island	32.55	64.70	36	359	British Admiralty [1977]
St. David's Island	32.37	64.65	34	355	British Admiralty [1977]
Great Sound	32.32	64.83	38	6	British Admiralty [1977]
St. George's Island	32.37	64.70	35	0	National Ocean Survey [1942]
St. George's Island	32.40	64.70	37	0	Perkeris and Accad [1969]
St. George's Island	32.37	64.70	36	359	Zahel [1970]
St. George's Island	32.40	64.70	36	358	Zettler et al. [1975]
Deep Sea (GOBI IV)	32.29	64.50	38	11	J. T. Kuo (personal communication, 1977)
Deep Sea (GOBI IV)	32.02	64.43	36	358	F. D. Malone (personal communication, 1978)

Here ξ is the tidal amplitude, and δ is the tidal phase relative to Greenwich.

blowing
ined for
the time-
t by (6).
theoretically,
ively, at
ediction
(8)

1. Of course, in regions of sufficiently small amplitudes, any phase error is acceptable.

At this point it must be mentioned that in shallow coastal areas of rapidly varying ocean tides, nonlinear hydrodynamical effects may be significant and must be accounted for in one way or another (section 4c). There one must remember that any nonlinearity generates higher harmonic frequencies and causes involved interactions between different tidal modes and also other ocean currents. In this connection, one may compare the introductory remarks to the *British Admiralty* [1977] tide tables.

b. Empirical Methods

Over many years, massive tidal records have been taken with about 10,000 tide gauges placed around the world at continental and island stations. Some of these records contain tidal time sequences longer than half a century with more than 10 million hourly readings. In recent years, *Eyries* [1968], *Snodgrass* [1968], *Filloux* [1969], and others developed sensitive deep-sea tide (pressure) gauges that can be placed almost anywhere on the ocean floor to record tidal variations for up to 1 year. Such deep-sea instrument packages measure also tidal current velocities, water temperatures, and other oceanographic quantities.

Most of the voluminous data banks have been harmonically analyzed by classical least squares methods in order to extract the important time-independent amplitudes and phases of the leading oceanic partial tides. The results have been collected and are now available from, for instance, the *National Ocean Survey* [1942], the *International Hydrographic Bureau* [1966], and the *British Admiralty* [1977]. Unfortunately, the so-called 'harmonic' analysis is not equivalent to a rigorous Fourier analysis and hence is affected by subjective and controversial errors. In particular, the time sequences are noisy because of variable recording inaccuracies and other pelagic and atmospheric disturbances of the geoidal sea level. The non-harmonic spectrum of the total tide has no true fundamental period and consists of bands of closely clustered frequencies which are difficult to separate.

As is mentioned in the introduction to the *British Admiralty* [1977] tide tables, nonlinear interactions between tidal modes and other ocean currents may be strong and long lasting, especially in shallow coastal waters. Since rough tidal data are recorded uniformly in various corners of the world oceans (between Europe and the British Isles, Nova Scotia and Cape Cod, and China and Korea; also northwest of Australia, on the Patagonian shelf, at the mouth of the Amazon river, etc.), one cannot simply dismiss such data as false recordings of 'certain' unreliable stations. These data clearly reflect the highly turbulent (eddying) nature of the oceanic tidal currents and must be properly accounted for in any realistic tidal model (section 4c). Indeed, significant distortions and retardations (some more than 60°) of ocean tides have also been recognized by researchers [e.g., *Harris*, 1904; *Bogdanov*, 1961a, b; *Defant*, 1961; *Gallagher et al.*, 1971; *Luther and Wunsch*, 1975; and *Schwiderski*, 1978b, 1979b] (see Tables 4a and 4b) near isolated islands and island chains or ocean ridges such as the Caribbean, Hawaiian, and Aleutian ridges. As was demonstrated by *Schwiderski* [1978b, 1979b, section 5a], the latter deformations have a profound effect on the global shape of open ocean tides.

Most of the mathematical shortcomings of the classical har-

monic analysis can be considerably reduced by using sufficiently long tidal time sequences. However, with shorter observations, significant errors (especially in the phase constants) may be encountered (see Table 2). For example, *Irish and Snodgrass* [1972] mention the differences in the harmonic constants (e.g., 25° in the S_2 phase angle) which Radok arrived at by applying the harmonic analysis to two short (19 days in January and 11 days in May) tidal recordings taken by *Noye and Easton* [1967] at the same station on the shelf of southern Australia. Nevertheless, the great majority of the tide data listed, for example, in the most recent *British Admiralty* [1977] tables (see their introduction) probably permit a tide prediction with the 10-cm accuracy posed in section 1. Naturally, some discrepancies between different tabulations must be expected, but only surprisingly few were found by the author [*Schwiderski*, 1978b, 1979b] at island stations. In fact, to the author's pleasant surprise, almost all of the seemingly incoherent M_2 tidal data, recorded at numerous clustered and scattered islands of the world oceans, permitted an unexpectedly realistic hydrodynamical integration into one coherent tidal topography (section 5a). The high quality of the tidal observations and their analyses and recordings is also supported by more recent measurements reported, for instance, by *Luther and Wunsch* [1975] and K. Wyrtki (private communication, 1978) for the Pacific, which do not deviate significantly from available older listings.

As a partial project of the international working group mentioned in section 1, *Munk and Cartwright* [1966] introduced the so-called 'ocean response method' in order to analyze relatively short time records with sufficient accuracy. Though this method is basically nonharmonic, it too yields as its end product the most desired harmonic constants. The local time series of the ocean tide is considered as a convolution of the tide-generating potential and a transfer function (complex response weights) which is, a priori, not known and hence must be determined in an optimum sense [*Cartwright*, 1968, 1969; *Cartwright et al.*, 1969]. By using analyzed coastal reference stations, satisfactory results are being claimed for rather short recording times of 2 weeks and even 1 week. While such modern filter techniques can be very successful, they are highly subjective and sometimes controversial. In any case, they rely to a considerable degree on practical experience. In this respect the comparative studies conducted, for instance, by *Munk and Cartwright* [1966], *Nowroozi* [1972], *Larsen and Irish* [1975], J. T. Kuo (private communication, 1977), and F. D. Malone (private communication, 1978) (see Table 3) are most instructive.

Analyzed deep-sea tidal measurements have been published by *Munk et al.* [1970], *Irish et al.* [1971], *Irish and Snodgrass* [1972], *Nowroozi* [1972], *Moffeld* [1975], *Pearson* [1975a, b], *Zeitler et al.* [1975], *Larsen and Irish* [1975], *Gill and Porter* [1979], and others. Additional measurements are being accumulated on a continued basis by D. E. Cartwright (private communication, 1978) around the British Isles (see also *Cartwright* [1971, 1977]), J. T. Kuo (private communication, 1977), F. D. Malone (private communication, 1978), S. K. Gill and D. L. Porter (private communication, 1978), off the U.S. Atlantic coast, and K. Wyrtki (private communication, 1978) at Pacific islands. Some of the deep-sea M_2 tide data known to the author are listed in Table 3 (section 5a) or illustrated in Figure 3. A complete collection in book form of all open ocean tide data (about 108 stations) known today has been

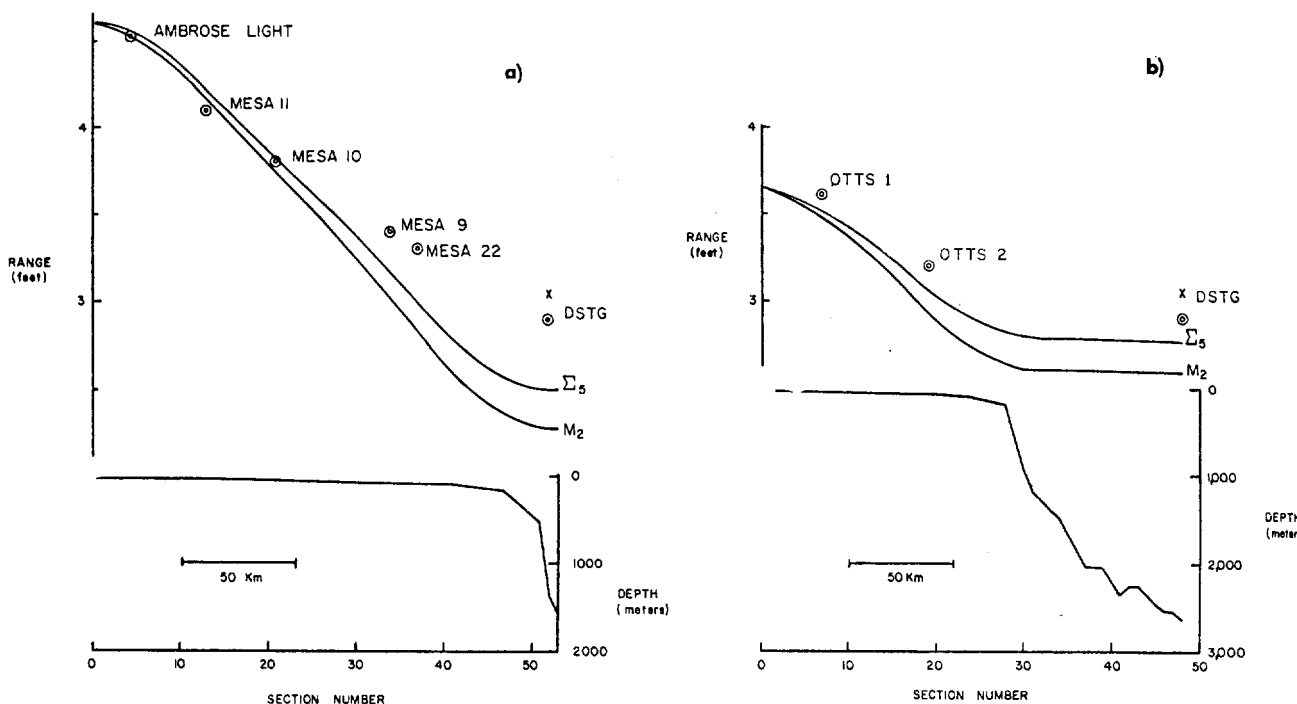


Fig. 3. Gill and Porter's [1979] profile measurements of decaying tidal ranges across a continental shelf. (a) Southeast of Sandy Hook, New Jersey. (b) Southeast of Bethany Beach, Delaware. The curve labeled M_2 is the Defant shelf model, and that labeled Σ_5 is the Gill-Porter shelf model. Crosses indicate the Schwiderski global model (average cell value (see Table 4a)).

prepared by Cartwright *et al.* [1979]. Finally, a large collection of coastal tide data around the islands of Japan compiled by Miyazaki *et al.* [1967] must be mentioned here.

By simple inspection of numerous observed ocean tide data and experienced intuition, 'cotidal' (equiphase) and some 'corange' (equiamplitude) maps have been constructed for marginal seas and partial or worldwide oceans by Whewell [1833, 1848], Berghaus [1845], Harris [1904], Sterneck [1920, 1921], Dietrich [1944a, b], Villain [1952], Bogdanov [1961a, b], Luther and Wunsch [1975], and others. All of these maps give a qualitative overview of the phenomena of ocean tides, and some of them have achieved a remarkable degree of reality, at least in certain ocean areas.

A more systematic empirical method to map large-scale ocean tides was proposed and demonstrated by Kuo *et al.* [1970a, b, 1977] and Jachens and Kuo [1973]. In their 'inversion method,' modern optimization techniques are utilized to fit low-degree polynomials simultaneously to observed ocean tide data and to measured oceanic tidal disturbances of the solid earth gravity field, which are correlated through well-known interaction equations. While this approach is definitely more reliable than purely intuitive attempts, it appears to be constrained by rather low-degree polynomials, which can hardly accommodate the various tidal undulations known from observations (section 5a). The method offers no physical insight into the tidal phenomena and yields no information on tidal currents, which is needed in certain applications. Aside from these shortcomings the method seems to yield promising results in limited ocean regions.

Open ocean measurements of tides are obviously of significant value to empirical and theoretical tide models, either as input or solely as calibration data. Future measurements should be encouraged, particularly in areas of high tidal amplitudes and even more in arctic and antarctic regions, where

reliable measurements of tides (and depths) are sparse. Recently, Gill and Porter [1979] reported on the first profile measurements of tidal decay from shallow shore points to the edge of the continental shelf. They confirmed experimentally the long-believed drastic decay of tidal heights (Figure 3) downward on continental shelves. Precisely the same important phenomenon has been brought out independently by the author's hydrodynamical interpolation technique (see sections 4c and 5a, Schwiderski 1978b, 1979b), and Tables 4a and 4b). Clearly, more profile measurements of the same Gill-Porter type are needed (between Cape Cod and Nova Scotia, at the mouth of the Amazon river, on the Patagonian shelf, etc.) to improve and/or check the accuracy of tide models.

c. Elementary Solutions of Laplace's Tidal Equations

Although Newton [1687] clearly recognized the distinctly hydrodynamical nature of ocean tides, it was Laplace [1775] who formulated the first hydrodynamical equations of ocean tidal motions. The 'Laplace tidal equations' (LTE's) can be written in the form

$$U_r = \frac{GH}{R \sin \theta} (\eta - \zeta)_\lambda + 2\Omega V \cos \theta \quad (18a)$$

$$V_r = \frac{GH}{R} (\zeta - \eta)_\theta - 2\Omega U \cos \theta \quad (18b)$$

$$\zeta_r + \frac{1}{R \sin \theta} [U_\lambda - (V \sin \theta)_\theta] = 0 \quad (19)$$

by using the following notations in addition to those introduced in section 2a:

R radius of the earth, equal to 0.637×10^7 m;

Ω earth angular velocity, equal to 0.72722×10^{-4} s⁻¹;

H
(u, v)
(U, V)

These
'continu
detail b
eddy di
anic tida
viously
subject
forces g
potential
tidal mo
tidal hei
ally tacit
[1978b,

If one
quency
time dep

and arr

The r
single e
tidal am
colatitu

where re

Nume
lytic and
tuaries, a
well-kno
Ferrel [1
Lamb a
Doodson
[1974]. M
been col
Bartels,
1932; N
1960].

The e
LTE's, n
tions [Se
be verifi
(22)) fo
(H = H₀)

Semidiu

Diurnal t

- H (static) ocean depth, equal to $H(\lambda, \theta)$;
 (u, v) east north velocities;
 $(U, V) \approx$ (depth integrated) east and north velocities, equal to $H \cdot (u, v)$.

These equations can be obtained from the more complete 'continuous ocean tidal equations' (COTE's) derived in full detail by Schwiderski [1978b, 1979a] by simply neglecting all eddy dissipation, bottom friction, and all terrestrial and oceanic tidal load effects in (28) and (29). The LTE's consider obviously an inviscid, incompressible, and single-layer ocean subject only to linearized inertial, potential, and Coriolis forces generated by the primary astronomical tide-producing potential $G\eta$ specified by (1)–(4). Of course, since the oceanic tidal motion is highly turbulent, the velocity (U, V) and the tidal height ξ must be considered as 'averaged' in some (usually tacitly bypassed) sense (see section 3a and Schwiderski [1978b, 1979a]).

If one considers a single partial tide η specified by its frequency σ (equations (2)–(5)), one can eliminate the complex time dependence by the substitution

$$(\eta, \xi, U, V) = (\bar{\eta}, \xi, \bar{U}, i\bar{V})e^{i\sigma t} \quad (20)$$

and arrive at the complex amplitude equations

$$\sigma \bar{U} = \frac{iGH}{R \sin \theta} (\xi - \bar{\eta})_\lambda + 2\Omega \bar{V} \cos \theta \quad (21a)$$

$$\sigma \bar{V} = \frac{GH}{R} (\bar{\eta} - \xi)_\theta + 2\Omega \bar{U} \cos \theta \quad (21b)$$

$$\sigma \xi = \frac{1}{R \sin \theta} [i\bar{U}_\lambda + (\bar{V} \sin \theta)_\theta] \quad (22)$$

The reduced equations can obviously be combined into a single elliptic partial differential equation for the complex tidal amplitude ξ , which is everywhere regular except at the colatitudes θ determined by

$$\sin \theta = 0 \text{ (poles)} \text{ or } \cos \theta = \sigma/2\Omega \quad (23)$$

where regular solutions exist.

Numerous solutions of the LTE's were constructed by analytic and semianalytic methods for idealized ocean basins, estuaries, and channels. Realistic results were sought by many well-known researchers, such as Laplace [1775], Airy [1842], Ferrel [1874], Thomson [1879], Hough [1897], Poincaré [1910], Lamb and Swain [1915], Proudman [1915], Proudman and Doodson [1927], Platzman [1971, 1972a, b, 1975], and Miles [1974]. Most of this rich and sometimes controversial work has been collected and analyzed in many books and reviews [e.g., Bartels, 1957; Defant 1957; Fomin, 1964; Hopfsner, 1931; Lamb 1932; Neumann and Pierson, 1966; Stern, 1975; Stommel, 1960].

The enormous difficulties, that were encountered with the LTE's, may be displayed by the following elementary solutions [Schwiderski, 1978b, 1979a; Hendershott, 1972]. As can be verified by simple substitution, the equations ((21) and (22)) for a stationary earth ($\Omega = 0$) of globally constant depth ($H = H_0$) yield the following exact solutions:

Semidiurnal tides ($\nu = 2$)

$$\eta = K \sin^2 \theta e^{i(\sigma t+2\lambda)} \rightarrow \xi = -\hat{K}\eta \quad (24)$$

Diurnal tides ($\nu = 1$)

$$\eta = K \sin 2\theta e^{i(\sigma t+\lambda)} \rightarrow \xi = -\hat{K}\eta \quad (25)$$

Long-period tides ($\nu = 0$)

$$\eta = K(3 \sin^2 \theta - 2)e^{i\sigma t} \rightarrow \xi = +\hat{K}\eta \quad (26)$$

where

$$\hat{K} = 6GH_0/(\sigma^2 R^2 - 6GH_0) \quad (27)$$

These simple integrals exhibit the following important properties of ocean tides:

Regularity and long periodicity of arctic tides. Near the north pole, arctic tides are regular and essentially of the long-period species. This significant feature holds true even for dissipative oceans on the rotating realistic earth [Schwiderski, 1978b, 1979a].

Resonance catastrophe of Laplacian hydrodynamic tides. On a stationary or rotating earth, Laplacian hydrodynamic tides are subject to resonance catastrophes at certain depths.

Second tidal paradox [Lamb, 1932]. On a stationary earth of modest ocean depth, all Laplacian hydrodynamic tides are inverted, i.e., lag 180° behind the corresponding Newtonian equilibrium (static) tides.

The dramatic 180° turnaround of Newton's equilibrium tide (section 2a and Figure 1b) by the Laplacian hydrodynamic tide with an inherent resonance menace is perhaps the most stunning result of the classical theory of ocean tides. The controversy between high and low tides under the moon (or sun) was, of course, quickly resolved by empirical studies and by considering more realistic ocean basins on a rotating earth. Since the forced ocean tides cannot reverse themselves (section 2a), they were found rotating around so-called amphidromic points (section 5a, Table 4, and Figure 8) due to the presence of the continents and the Coriolis force. Nevertheless, as can be verified by comparing the recent tidal maps published by experimental and theoretical tidalists (see, for example, the review collections of Hendershott [1973, 1977]), the fundamental controversy between high and low tides over certain significant areas (north central Pacific, South Atlantic, etc.) persisted as hot as ever till today.

Naturally, in realistic ocean basins, no eigensolution of the LTE's (18) can exactly match the forcing equilibrium tide, which precludes any total resonance catastrophe. Nevertheless, in the Laplacian theory of tides 'near resonance' is possible at certain ocean depths of the real ocean basin. Indeed, numerical tidalists [e.g., Pekeris and Accad, 1969; Hendershott, 1972, 1975, Parke and Hendershott, 1979; Accad and Pekeris, 1978] using the LTE's without any dissipation terms (sections 3a–3c) clearly felt the resonance threats as instabilities of their numerical procedures.

3. MODELING CONTINUOUS OCEAN TIDAL EQUATIONS

a. Continuous Ocean Tidal Equations

The difficulties with the Laplacian hydrodynamical theory of tides (section 2c) can only be attributed to the oversimplified LTE's (18) and (19). Indeed, it is hard to see how to overcome the resonance threats at certain ocean depths without assuming an artificial ocean basin, including density stratification, allowing vertical motions [e.g., Lamb, 1932; Cartwright, 1977], or reintroducing the neglected nonlinear inertial and viscous forces. Obviously, the last possibility yields the most natural resolution of the problem at hand. In fact, it is well known today [e.g., Schwiderski, 1972] that while nonlinear inertial forces cause instabilities and turbulence in

viscous fluid motions, they also control them and prevent any kind of catastrophe by generating sufficient Reynolds stresses or eddy dissipation.

Even without the resonance problems of the LTE's the necessity for appropriate eddy dissipation forces follows directly from the enormous dimensions of the world oceans in which tidal currents of all 'resolvable' wavelengths are supercritically turbulent. For example, a tidal motion of 0.01-cm²/s kinematic molecular viscosity, 100-km characteristic wave length (about 1° mesh size (section 4a)), and moderate characteristic velocity of 0.1 cm/s possesses a characteristic Reynolds number of 10⁸, which [e.g., Schlichting, 1968] is well in the turbulent flow regime. Accordingly, any comprehensive study of ocean tidal currents must augment the LTE's (18) by two additional vector terms modeling eddy dissipation and bottom friction.

In his study of tides in the Red Sea, Grace [1930a] introduced the effects of the solid earth tide into ocean tidal research (see also Munk *et al.* [1970], Hendershot and Munk [1970], and Cartwright [1971]). Recent gravity measurements [e.g., Kuo *et al.*, 1970a, b] revealed a significant interaction between the oceanic and terrestrial tides. In spite of such earlier studies it was Farrell [1972a, b, 1973] who suggested that accurate global tide models must account for the mutual disturbances exerted by the terrestrial tide on the oceanic tide and vice versa. Consequently, the primary astronomical tide-generating potential of the LTE's (18) must be extended to include two major additional terms representing secondary effects due to the terrestrial and oceanic tidal loads.

With the important extensions of the LTE's (18) mentioned above, one arrives at the following most general continuous ocean tidal equations ever used in theoretical tide models:

$$U_t = \frac{GH}{r \sin \theta} (\eta - \hat{\eta} - \zeta + \hat{\zeta})_\lambda + 2\Omega V \cos \theta + A^\lambda + B^\lambda \quad (28a)$$

$$V_t = \frac{GH}{R} (\zeta - \hat{\zeta} - \eta + \hat{\eta})_\theta - 2\Omega U \cos \theta + A^\theta + B^\theta \quad (28b)$$

$$R \sin \theta \zeta, U_\lambda - (V \sin \theta)_\theta = 0 \quad (29)$$

In these COTE's the notations of the considerably simpler LTE's (18) and (19) are retained with the following additions:

- (A^λ, A^θ) lateral dissipation vector (to be modeled in section 3b);
- (B^λ, B^θ) bottom friction vector (to be modeled in section 3c);
- $\hat{\eta}, \hat{\zeta}$ terrestrial and oceanic tidal-load potentials, respectively (to be modeled in section 3d).

A formal complete derivation of the COTE's (28) and (29) from the Navier-Stokes equations of 'averaged' turbulent flow [e.g., Schlichting 1968; Whitaker, 1968] is given by Schwiderski [1978b, 1979a]. It suffices here to mention only the most important assumptions and simplifications.

1. The sea surface at rest is assumed to be perfectly spherical without any geoidal undulations or atmospheric and density-driven disturbances.

2. The ocean floor at rest is specified by some averaged (section 4a) bathymetry subject to perturbations due to the astronomical equilibrium tide and to the oceanic tidal load (section 3d).

3. The averaged turbulent velocity components and tidal height (or fluid pressure) are considered as some sort of 'generalized quantities,' which in their discrete form (section 4b)

are physically defined as mean values ('divided mass fluxes') over some lateral or horizontal mesh cell area $\Delta s (>0)$ and time interval $\Delta t (>0)$. The area Δs and the time step Δt must be chosen in an optimum way to allow for a sufficient resolution of all significant wavelengths and tidal periods.

4. The 'stresslike' effects (Reynolds stresses) of the turbulent 'velocity fluctuations' (filtered-out velocity residuals) on the mean flow must be modeled as lateral eddy dissipation (section 3b) and bottom friction (section 3c) to achieve a macroscopically unique and physically realistic description of the microscopically undetermined turbulent motion under consideration.

5. The hydrostatic pressure assumption is invoked; that is, all quadratic inertial terms, centrifugal accelerations, vertical Coriolis and dissipation forces, and vertical motions are neglected.

6. A single-layer ocean is assumed; that is, because of the depth-independent driving body force, all velocity components are considered to be essentially depth independent.

Attention to the important concept of averaged velocities and tidal height (assumption 3) was drawn by the author [Schwiderski, 1978b, 1979a]. It was argued that the COTE's possess only a vague formal meaning, which helps the numerical analyst to set up mathematically well-defined finite-difference equations (section 4). In those physically approximate but sound discrete ocean tidal equations, all velocities and tidal elevations are rigorously defined as mass fluxes through mesh cell areas Δs during the time interval Δt divided by Δs , Δt , and the corresponding density. Obviously, in contrast to laminar flows the averaged turbulent flow variables depend strongly on the considered values Δs and Δt . The larger Δs and Δt are chosen, the more and larger fluctuating or eddying motions are filtered out from the remaining mean motions. Although the COTE's should always be recoverable from the finite-difference analog by a formal limit process, even in general laminar flows these limits must be understood in some generalized (distribution) sense [e.g., Ladyzhenskaya, 1969] with no pointwise meaning. Therefore the main effort of modeling oceanic tidal motions must focus primarily on the discrete ocean tidal equations (DOFE's) (60) and (61), which should represent the true macroscopical effects of the Reynolds stresses as closely as possible.

b. Lateral Eddy Dissipation

As was mentioned in section 3a, the COTE's (28) and (29) are derived from the Navier-Stokes equations of formally averaged turbulent flow. These equations contain the so-called Reynolds stress tensor [e.g., Schlichting, 1968] in which the velocity fluctuations (filtered-out residuals) manifest their influence on the remaining mean velocity. In spite of an enormous research effort of more than a century this stress tensor remains unknown. Obviously, it reflects the microscopically undetermined nature of turbulent motions, which has been pointed out, for example, by Schwiderski [1978b, 1979a].

Modern experiment [e.g., Busse and Whitehead, 1971] and mathematical [e.g., Schwiderski, 1972] research has clearly established that in the critical regime, laminar and turbulent motions are no longer uniquely determined by laminarlike differential equations and initial, boundary, and regularity conditions. The occurring motions appear to be governed by hysteresis and pure chance. Also, since the product of generalized (distribution) functions has no mathematical meaning [e.g., Shilov, 1968], there seems to exist 'no meaningful ordi-

nary or
Reynold
mined fl

Never
filtered-
ically qu
macrosc
forces a
mechan
Reynold
changing
viscosity
phy this
man [19
[see Mu
currents
been pic
be name
rect rele
[1963],
[1968],
schman
[1975]. I
neered th
viscosity
der [196
as well a
al. [1969]

Ignori
some res
In the ab
the phys
fact rema
tion incl
searcher:
Boussine
test in m
ography,
is no exc

Appar
stitution
eddy visco
investiga
viscosity
viscositie
[Cox, 19
the eddy
low), an
been disc
terest to
large var
tion by A
tidal mo
extensive
well-known
Navier-S
viscosity.

As was
a charact
tigation a
viscosity.
the macr
undefined

nary or generalized function that could possibly represent the Reynolds stress tensor which contains the pointwise undetermined fluctuating velocity residuals in quadratic form.

Nevertheless, the energy-dissipating stresslike effects of the filtered-out velocity fluctuations on the average flow are physically quite apparent and hence must be modeled in some macroscopical sense. The first model of such interior friction forces acting in a turbulent motion was introduced into fluid mechanics by Boussinesq [1877], who replaced the unknown Reynolds stress tensor by the known laminar stress tensor, changing only the molecular viscosity to the so-called 'eddy viscosity' with its magnitude at one's disposal. In oceanography this simple substitution was brought into practice by Ekman [1902] and was later effectively used by Munk in 1950 [see Munk, 1963]. In numerical modeling of general ocean currents and atmospheric circulations the Boussinesq idea has been picked up by many researchers, of whom only few may be named here because their important contributions with direct relevance to ocean tides: Bryan [1963], Smagorinsky [1963], Friedrich [1966, 1970], Crowley [1968, 1970], Leith [1968], Cox [1970], O'Brien [1971], and Holland and Hirschman [1972] as well as Döös *et al.* [1974] and Reid *et al.* [1975]. In numerical ocean tidal modeling, Hansen [1966] pioneered the use of lateral eddy dissipation with a constant eddy viscosity. He was soon followed by his co-workers Bretschneider [1967], Trepka [1967], and Zahel [1970, 1973, 1975, 1977] as well as by other independent workers such as Marchuk *et al.* [1969], Marchuk *et al.* [1973], and Estes [1975, 1977].

Ignoring the successes of Boussinesq's unique approach, some researchers still regard it as fictitious and controversial. In the absence of better solutions it seems idle to argue about the physical justification of the Boussinesq substitution. The fact remains that it represents the simplest constitutive equation including zero used 'artificially' by some objecting researchers. Above all, as with any other physical law, the Boussinesq eddy dissipation has successfully passed its crucial test in many practical applications in hydrodynamics, oceanography, and meteorology. The present oceanic tidal motion is no exception (see section 5a).

Apparently, the reluctant acceptance of the Boussinesq substitution originates from the observation that the 'constant' eddy viscosity varies enormously in form and magnitude from investigator to investigator. While the kinematic molecular viscosity of water is of the order of 10^{-2} cm²/s, oceanic eddy viscosities of the order of 10^0 to 10^{11} cm²/s have been quoted [Cox, 1970; Zahel, 1970]. Nevertheless, the huge variation of the eddy viscosity is physically plausible (see discussion below), and some empirical evidence for the lower value has been discussed by Munk [1966]. In this connection it is of interest to know that the mean flow is quite insensitive to fairly large variations (say, 25%) of the eddy viscosity. This observation by Munk and Palmén [1951] was confirmed for oceanic tidal motions by the author's [Schwiderski, 1978b, 1979a, b] extensive computer experiments. It is probably related to the well-known fact that potential motions satisfy the complete Navier-Stokes equations of laminar flow with any constant viscosity.

As was first realized by Prandtl [1925], the eddy viscosity is a characteristic quantity of the turbulent motion under investigation and not just a fluid constant such as the molecular viscosity. In fact, a prescribed eddy viscosity actually specifies the macroscopical (averaged) features of the microscopically undefined turbulent flow. Consequently, the quality of the

modeling of any turbulent motion is directly linked to the investigator's realistic choice of the eddy viscosity. The Boussinesq substitution permits the analyst to choose a suitable velocity-dependent or velocity-independent eddy viscosity either uniformly or separately for all three stress directions. If the velocity field were known a priori, then one could determine exact eddy viscosities a posteriori in many ways.

The physically sound meaning of Boussinesq's approximation of the Reynolds stresses was first illustrated by Prandtl's [1925] celebrated 'momentum austausch (exchange, mixing) theory' of turbulent flow. With the help of constant 'mixing-length parameters' [e.g., Schlichting, 1968] the eddy viscosity (momentum austausch coefficient) is found to be dependent on the averaged flow velocity; that is, the eddy dissipation appears as a quadratic phenomenon. In meteorology and oceanography, velocity-dependent eddy viscosities were derived or physical grounds by Smagorinsky [1963], Leith [1968], Crowley [1968, 1970], O'Brien [1971], and others.

The author's [Schwiderski, 1978b, 1979a] early computer experiments with a worldwide, constant eddy viscosity in an ocean of depth varying from 10 to 7000 m clearly indicated that the lateral eddy viscosity must depend linearly on the ocean depth. Eddy viscosities depending on $\frac{1}{2}$ and $\frac{3}{2}$ powers of the depth were also tried, but they failed to yield equally good results. A renewed look at the phenomenon of turbulent motion led to the introduction of a lateral eddy viscosity that depends linearly on a horizontal (cell or mesh size) and a vertical (cell size or depth) mixing length. In view of the planned grid discretization of the spherical ocean area a lateral eddy viscosity was defined by

$$A = (a/2) LH(\lambda, \theta)(1 + \mu \sin \theta) \quad (30)$$

where a is the reduced eddy coefficient (in s⁻¹), L is the chosen equatorial mesh length, and μ is the longitudinal grading parameter chosen to achieve more uniform spherical mesh areas (section 4a).

As is physically plausible, the novel eddy viscosity A depends on the mean lateral cross-section area

$$\Delta s = HL(1 + \mu \sin \theta)/2 \quad (31)$$

of the local flow cell of depth H . Since the mean tidal velocities in the discrete tidal equations (equation (60) and (61)) depend strongly on the mesh area Δs (see section 3a), the assumed dependence of A on Δs is physically well justified. Indeed, larger Δs values mean that more fluctuating or eddying motions are filtered out from the mean velocity, which results in more vigorous eddy dissipation. Also, in agreement with physical expectations one concludes from (30) that eddy dissipation is significant in deep ocean basins and negligible in shallow shelf regions. The remaining reduced eddy coefficient a depends probably in some way on the discrete time step Δt (section 3a). However, in any particular application, Δt is necessarily a constant, so that a remains to be determined, say, as a uniform constant over all oceans by trial and error to achieve best agreements with observations. In the author's tide model with a bathymetry varying from 10 to 7000 m the eddy viscosity varied as follows:

$$1.3 \cdot 10^3 < A < 1.3 \cdot 10^6 \text{ m}^2/\text{s} \quad (32)$$

which fits the customary range mentioned above very well. Thus the viscosity law (30) explains the huge magnitude differences in the constant eddy viscosity used by numerical analysts in different problems. The fact that the eddy viscosity

must depend in some way on the mesh size (resolution) in discrete models of ocean currents was earlier noticed by Cox [1970], Friedrich [1970], Holland and Hirschman [1972], and Zahel [1975].

By applying assumptions 1–6 of section 3a to the Boussinesq substitution with the eddy viscosity specified by (30) one arrives [Schwiderski, 1978a, 1979a] at the lateral eddy dissipation terms of the COTE's (28) and (29):

$$\begin{aligned} A^\lambda = \frac{A}{R^2} & \left[\frac{U_{\lambda\lambda} + \bar{H}_\lambda U_\lambda}{\sin^2 \theta} + U_{\theta\theta} + (\cot \theta - \bar{H}_\theta + \bar{H}_\theta) U_\theta - H^\lambda U \right] \\ & + \frac{A}{R^2 \sin \theta} [\bar{H}_\lambda \bar{H}_\theta V - (2 \cot \theta + \bar{H}_\theta) V_\theta] \end{aligned} \quad (33a)$$

and

$$\begin{aligned} A^\theta = \frac{A}{R^2} & \left[\frac{V_{\lambda\lambda}}{\sin^2 \theta} + V_{\theta\theta} + (\cot \theta - \bar{H}_\theta + 2\bar{H}_\theta) V_\theta - H^\theta V \right] \\ & + \frac{A}{R^2 \sin \theta} [2 \cot \theta U_\lambda - \bar{H}_\lambda U_\theta - (\cot \theta - \bar{H}_\theta) \bar{H}_\lambda U] \end{aligned} \quad (33b)$$

where

$$\begin{aligned} H^\lambda = \frac{\bar{H}_{\lambda\lambda} + 1 + H_\lambda^2}{\sin^2 \theta} & + \bar{H}_{\theta\theta} - \bar{H}_\theta (\bar{H}_\theta - \bar{H}_\theta) \\ & + (\bar{H}_\theta + \bar{H}_\theta) \cot \theta \end{aligned} \quad (34a)$$

$$H^\theta = \frac{\bar{H}_{\lambda\lambda} + 1}{\sin^2 \theta} + \bar{H}_{\theta\theta} + \bar{H}_\theta (\cot \theta - \bar{H}_\theta + 2\bar{H}_\theta) \quad (34b)$$

$$\bar{H}_\theta = H_\theta / H \quad \bar{H}_{\theta\theta} = H_{\theta\theta} / H \quad \theta \rightarrow \lambda \quad (35)$$

$$\bar{H}_\theta = \bar{H}_\theta + \mu \cos \theta / (1 + \mu \sin \theta) \quad (36)$$

These equations include all lateral eddy dissipation terms used so far in ocean tidal models. In particular, for $A = \text{const}$, instead of (30) one obtains the considerably simpler terms used by Hansen [1966], Zahel [1970, 1973, 1975, 1977], Marchuk et al. [1973], Estes [1975, 1977], and others. Of course, for $A = 0$, all eddy dissipation is wiped out, as occurs in the COTE's used by most numerical tidalists, such as Hansen [1948, 1949], Pekeris and Accad [1969], Hendershot [1972, 1975], Parke and Hendershot [1979], and Accad and Pekeris [1978]. It may be mentioned that the author's [Schwiderski, 1978b, 1979a, b] extensive computer experiments clearly demonstrated best results for the eddy viscosity law specified by (30) instead of $A = 0$ or $A = \text{const} > 0$.

c. Bottom Friction Laws

Through the integration of the simplified Navier-Stokes equations with the Boussinesq replacement of the Reynolds stress tensor (sections 3a and 3b) carried out over the depth of the single-layer ocean, one arrives (see Schwiderski [1978b, 1979a] for full details) at the bottom friction vector (B^λ, B^θ) entering in the COTE's (28). This stress vector depends directly on the vertical eddy viscosity and is, of course, not known. However, on the basis of hydrodynamical research on wall friction [e.g., Schlichting, 1968] the substitutions

$$B^\lambda = -Bu = -BU/H \quad U = Hu \quad (37a)$$

and

$$B^\theta = -Bv = -BV/H \quad V = Hv \quad (37b)$$

have been widely accepted in many successful applications. Similarly to the eddy viscosity (section 3b) the following velocity-independent and velocity-dependent 'bottom friction coefficients' B have been considered:

'Linear law' of bottom friction

$$B = \text{const in velocity } (u, v) \quad (38)$$

'Quadratic law' of bottom friction

$$B = \gamma(u^2 + v^2)^{1/2} = \gamma(U^2 + V^2)^{1/2}/H \quad (39)$$

where the values of B or γ , respectively, remain at one's disposal.

While the quadratic law is suitable for general (fast) motions, the linear law is appropriate only for so-called Stokes slow motions [e.g., Schlichting, 1968]. In fluid mechanics the physical significance of the quadratic law of wall friction was first pointed out by Boussinesq [1896]. Later, Taylor [1918] applied it advantageously in his study of tidal currents in the Irish Sea. Following Taylor the quadratic law of bottom friction was used in numerical modeling of ocean tides by Hansen [1966], Zahel [1970, 1973, 1975, 1977], Marchuk et al. [1973], Estes [1975, 1977], and others.

In order to retain the linearity of the tidal equations for their adopted time-independent numerical procedure, Pekeris and Accad [1969] used the linear law of bottom friction with a coefficient depending inversely on the ocean depth. These authors also called attention to the earlier work by Grace [1930b], who applied both the quadratic and the linear law of bottom friction to the problem of the tides in the Gulf of Suez. Grace experienced a slight preference for the linear law. Similarly to eddy dissipation (see discussion above) it appears that the linear law of bottom friction is more consistent with all other assumed linearizations of the equations of slow (Stokes-like) averaged tidal motion. Furthermore, the convergence characteristics of the time-stepping computations carried out and displayed by Estes [1975] with the quadratic law of bottom friction fail to exhibit any nonlinear symptoms.

On the basis of the earlier studies mentioned above, the author [Schwiderski, 1978b, 1979a] adopted the linear law of bottom friction as being preferable at least in open ocean areas. However, in contrast to the results of Pekeris and Accad [1969], the bottom friction coefficient was experimentally found to be more realistic without any dependence on the ocean depth. The depth-dependent coefficient chosen by Pekeris and Accad [1969] was evidently justified in their ocean basin, cut off artificially at the 1000-m depth level. Since turbulent flows display only a very thin boundary layer, a depth-independent friction coefficient is appropriate in an ocean of depth varying from 10 to 7000 m. As can be seen from the right-hand form of equations (37) with a constant B , bottom friction in the COTE's (28) decreases inversely with the first power of the depth H and becomes negligible in deep oceans. In the case of Pekeris and Accad the influence of bottom friction decreases inversely with the second power of the depth H , which is far too rapid in the 10- to 500-m depth range.

As was mentioned above, the bottom stress depends directly on the vertical eddy viscosity; hence a depth-independent bottom friction coefficient in equations (37) is consistent with the physical arguments presented in section 3b concerning eddy viscosities in discrete flow models. In complete analogy with those discussions the bottom friction coefficient B in equations

Fig. ...
earth tide
the earth

(37) sh
area

i.e.,

where ...
duced ...
error co...
cient B
1978b,
constant
observe
model c
duced v

The ...
form B
Other ...
and M
the aut...
shallow...
must be
4c).

d. Sec

All e
nomica
ponent.
Farrell
actions
be incl
and de
tide-m
elastic
oceanic

In m
sidered
the ear
tide η
total o
the equ

Acco
COTE'

(due to

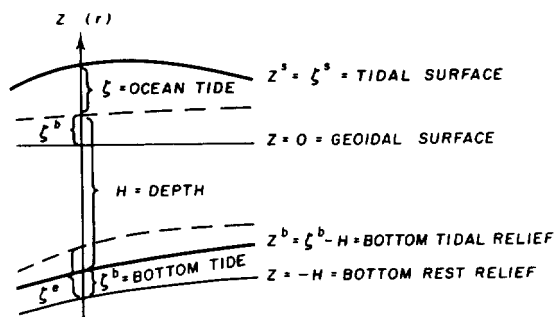


Fig. 4. Earth-ocean tidal interaction: ζ is the ocean tide. ζ^e is the earth tide, ζ^s is the surface tide. ζ^b is the bottom tide, $\zeta^{eo} = \zeta^e - \zeta^b$ is the earth dip response to the ocean tide, and H is the ocean depth.

(37) should depend linearly on the average bottom mesh cell area

$$\Delta s = L^2 \mu \sin \theta \quad (40)$$

i.e.,

$$B = bL^2 \mu \sin \theta = b\mu \sin \theta \quad (41)$$

where L and μ are defined in section 3b. The remaining reduced friction coefficient b must be determined by trial-and-error computations for best results. The new friction coefficient B (equation (41)) was used by the author [Schwiderski, 1978b, 1979a, b] with only minor advantages over a simply constant B . At this point it may be mentioned that the author observed a considerably stronger dependence of the tidal model on the value chosen for b than on the corresponding reduced viscosity coefficient a of section 3b.

The author tested also bottom friction coefficients of the form $B \sim H^\epsilon$ with $\epsilon = \frac{1}{2}, -\frac{1}{2}, -1, -\frac{3}{2}$ but with poorer results. Other bottom friction laws were considered by Johns [1966] and McGregor [1972], as well as by Kagan [1971, 1972]. From the author's computer experiments it was concluded that in shallow ocean areas, certain nonlinear bottom friction effects must be considered in addition to the linear law used (section 4c).

d. Secondary Tide-Generating Forces

All earlier numerical tidalists used only the primary astronomical equilibrium tide η (section 2a), mostly the M_2 component, for the driving force of global ocean tides. Recently, Farrell [1972a, b, 1973] called attention to significant interactions between the oceanic and terrestrial tides, which should be included in accurate ocean tide models. Farrell went on and derived the mathematical expressions of those secondary tide-modifying forces, assuming a dissipationless perfectly elastic earth subject to the astronomical body force and the oceanic tidal surface load.

In more detail the following five interaction effects are considered to be significant (see Figure 4): (1) $\zeta^e, \zeta^{eo} = \zeta^e - \zeta^b$ are the earth tidal responses due to the astronomical equilibrium tide η and the oceanic tidal load ζ , respectively where ζ^b is the total ocean bottom tide; (2) $\eta^e, \eta^{eo}, \eta^o$ are the perturbations of the equilibrium tide η in response to ζ^e, ζ^{eo} , and ζ , respectively.

According to their causes these perturbations enter in the COTE's (28) in the following grouped form:

$$\hat{\eta} = \zeta^e - \eta^e \quad (42)$$

(due to η) and

$$\hat{\zeta} = \eta^o + \zeta^{eo} - \eta^{eo} \quad (43)$$

(due to ζ). If η_n and ζ_n denote the n th-degree spherical harmonic components corresponding to η and ζ , then one has [after Farrell, 1972a]

$$\eta = \sum_n \eta_n \rightarrow \hat{\eta} = \sum_n (h_n - k_n) \eta_n \quad (44)$$

and

$$\zeta = \sum_n \zeta_n \rightarrow \hat{\zeta} = 3\alpha' \sum_n \frac{1 - h_n' + k_n'}{2n + 1} \zeta_n \quad (45)$$

where $\alpha' \approx 0.18$ denotes the ratio between the mean densities of the ocean water and the earth. The constant coefficients (h_n, k_n) and (h_n', k_n') are called Love numbers corresponding to (ζ^e, η^e) and (ζ^{eo}, η^{eo}).

Farrell derived some of the Love numbers on the basis of the Gutenberg-Bullen A earth model. Pekeris (in a presentation given in 1977 at the U.S. Office Naval Research) criticized Farrell's approach and went on to determine two new sets of Love numbers, one based on the Gutenberg and the other on the Dziewonski-Hales-Lapwood earth model [Accad and Pekeris, 1978]. However, all three sets display only minor differences which can be ignored in the present application.

Since all significant tidal species (section 2a) are purely spherical harmonics of degree $n = 2$, (44) reduces to

$$\hat{\eta} = 0.31\eta \quad (46)$$

where $h_2 - k_2 \approx 0.31$ in agreement with all three models of Farrell and Pekeris and Accad. This simple relationship reflects the drastically simplified properties of the earth model, which has been used to derive the representations for $\hat{\eta}$ and $\hat{\zeta}$ in (44) and (45) containing only real constant Love numbers. In particular, it has been assumed that lateral variations in the earth are negligible and that the terrestrial deformations (ζ , ζ^{eo}) and the gravity perturbations ($\eta^e, \eta^{eo}, \eta^o$) are all instantaneous responses to their causes η or ζ .

Equation (46) constitutes a significant 31% modification of the tide-generating forces in the COTE's (28), which definitely cannot be dismissed. Starting with Hendershot [1972], this correction has probably been included in all subsequent global tidal studies. All earlier linear or almost linear tide models [e.g., Pekeris and Accad, 1969; Zahel, 1970] with homogeneous boundary data (section 4c) can be corrected for this oversight by reducing all amplitudes with the uniform factor $\alpha = 1 - 0.31 = 0.69$. No adjustments of the phases are necessary.

The second correction $\hat{\zeta}$ (equation (45)) to the tide-generating forces in the COTE's (28) requires the knowledge of the oceanic tide ζ decomposed into its spherical harmonic components ζ_n . Assuming (for the moment) the a priori knowledge of ζ then one still faces a rather formidable numerical problem. The expansion of ζ must be carried out over the 'orthogonal range' of the spherical harmonics, that is, over the entire sphere with $\zeta = 0$ at land points. Thus, if a $1^\circ \times 1^\circ$ grid system (section 4a) is considered, 6.48×10^4 Fourier coefficients must be computed on 6.48×10^4 points to fit exactly all numerical ζ values. Since in practical computations only very few Fourier coefficients can be carried, the actual expansions of ζ and $\hat{\zeta}$ brush over all detailed features of the oceanic tide ζ (section 5a) and its response $\hat{\zeta}$. Moreover, no matter how many finite terms are being carried, the resulting ζ expansion is always contaminated with the well-known Gibbs phenomenon and yields only a generalized (δ type) derivative which is pointwise

meaningless. These difficulties were experienced by *Estes* [1979], who expanded his tidal model into spherical harmonics and found poor agreement with the original numerical tide data.

Owing to the denominator $(2n + 1)$, the expansion for ξ in (45) is absolutely convergent and yields ordinary derivatives as required by the COTE's (28). However, the expansions of those derivatives possess the same convergence and Gibbs phenomenon features as the oceanic tide ζ mentioned above. Using their own so-called zero-order tidal models of ζ , computed without the tidal loading effect ξ , *Hendershott* [1972, 1975], *Estes* [1977], *Zahel* [1977], and *Accad and Pekeris* [1978] evaluated by the equivalent (47) the response ξ and its partial derivatives. Although rather crude approximations were used, the results confirmed the original observations by Hendershott: the secondary loading effect ξ exceeds pointwise more than 50% of the primary equilibrium tide η , and its partial derivatives assume extremely large values compared to those of η . This seemingly stunning result lead to the prediction of huge ocean tidal loading effects on the oceanic tide. That puzzling experience was further enhanced when *Hendershott* [1972] included the estimated ξ in his COTE's ((28) with $A = B = 0$) and constructed a new 'first-order' oceanic tide ζ' , which differed drastically from the 'zero-order' tide ζ . A similarly unexplained result was recently reported by *Accad and Pekeris* [1978].

In an attempt to solve his COTE's with ocean loading effects ξ , *Hendershott* [1975] repeated his iteration step described above and computed successively ξ , ξ , ξ' , ξ'' , ξ''' , ... in an alternating procedure that failed to converge. In contrast, *Accad and Pekeris* [1978] followed Hendershott's iteration for a few steps and found no divergence symptoms. These opposing results are mathematically most interesting because both models use the same COTE's (28) and (29) without any eddy dissipation ($A = 0$) and bottom friction ($B = 0$) and employ a similar time-independent numerical method (section 4).

The first successful iterative solution of the COTE's (28) and (29) including all terms A , B , $\dot{\eta}$, and ξ was accomplished by *Estes* [1977] and *Zahel* [1977], who employed the well-known *Hansen* [1966] time-dependent numerical method (section 4). Both authors experienced no symptoms of divergence in their iteration. A similar result was reported by *Gordeyev et al.* [1977]. In order to overcome Hendershott's difficulties, *Parke and Hendershott* [1979] and *Parke* [1978] abandoned the search for an 'ordinary solution' of their COTE's and succeeded in finding a 'mean or weak' solution of these equations. Using earlier successive iteration solutions of ξ (converging or diverging) as base (called test) functions in a weighted linear superposition [*Hendershott*, 1977], they determined the weighting coefficients by fulfilling the COTE's or by matching empirical tide data in the mean. However, the quality of such modern mean solutions as ordinary solutions was not elaborated. Such an evaluation would be of great interest to numerical analysts, especially since only relatively few base functions have been used, which were permitted to diverge.

In order to understand the major mathematical difficulties involved in the above mentioned iterations the practical computation of the ocean loading effects ξ from a known oceanic tide ζ (equations (45)) may be illustrated here in somewhat more detail. By introducing the well-known integral definition of the Fourier coefficients of ζ one finds the following integral

representation for ξ (equations (45)) [*Farrell*, 1972a]:

$$\xi(\lambda, \theta) = \int \int_{\Sigma} G(\lambda', \theta'; \lambda, \theta) \xi(\lambda', \theta') \sin \theta' d\lambda' d\theta' \quad (47a)$$

with the 'kernel (called Green's) function'

$$G(\lambda', \theta', \lambda, \theta) = \frac{3\alpha'}{4\pi} \sum_n (1 - h_n' + k_n') P_n(\cos \theta) \quad (47b)$$

where Σ denotes the entire sphere, P_n the conventional Legendre polynomial of degree n , and θ the angular spherical distance between the points (λ, θ) and (λ', θ') .

In his presentation (see discussion above), Pekeris pointed out that the series of the kernel function (equation (47)) is only conditionally (not absolutely) convergent and yields no ordinary (only δ type) derivatives. Hence the evaluation of ξ , ξ_λ , and ξ_θ depends strongly on the number of terms carried and on the order of summation, integration, and differentiation. In particular, the partial derivatives of ξ required in the COTE's (28) may be taken by (1) differentiating ξ numerically, (2) differentiating ξ analytically term by term, (3) differentiating G numerically, or (4) differentiating G analytically term by term. One concludes from the properties of the Fourier coefficients of ζ (see discussion above) that methods 1-3 are all mathematically pointwise acceptable. Method 1 can be expected to be fairly smooth without Gibbs phenomena. Methods 2 and 3 should produce rough values due to Gibbs phenomena. Method 4 is only correct in the generalized sense without any pointwise meaning.

With their important solutions, *Estes* [1977] and *Zahel* [1977] broke the incredible expectations attributed to the ocean loading term ξ in comparison to the equilibrium tide η (see discussion above). Their and all subsequent tidal models displayed only moderate modifications (see discussion below) of the corresponding models with omitted ocean loading effects ξ . A closer look at the COTE's (28) reveals that ξ could be compared to η or to ζ . Since ξ is produced by ζ (equations (45)), only the latter case is evidently appropriate. In the light of this comparison, ocean loading effects emerge (as physically plausible) as truly secondary effects in agreement with all computed models. In fact, *Accad and Pekeris* [1978] compared their zero-order solution ξ with the corresponding ζ and found (in agreement with all other models) that ξ amounted only to some ('secondary') 10% of ζ . Moreover, ζ and ξ displayed a very close agreement in their phases. These authors explained the moderate ocean loading effects by the observed close resemblance between the lateral features of ζ and ξ . In contrast to ζ or ξ the equilibrium tide η covers essentially the entire ocean (Figure 1b) and should not be compared to ξ , which (although it is relatively large pointwise) is significant only within its amphidromic rotation systems similar to those shown in Figure 8 for the author's tide model. In other, more drastic, words, a high fountain of small diameter has little influence on the oceanic tide at large.

In order to avoid all mathematical difficulties involving the practical computation of the ocean loading term ξ , Pekeris in his presentation (see discussion above) suggested the simple relationship

$$\xi = \beta \zeta + \Delta \quad (48)$$

on the basis of his observed resemblance between ζ and ξ . With $\Delta = 0$ this relationship obviously can be argued physically just as well as the analogous relation of (46). Treating Δ as being negligible, Accad and Pekeris [1978] determined the constant β in the mean by an iteration procedure that converged to

$$\beta = 0.085 \quad (49)$$

Following this ingenious approach, the author [Schwiderski, 1978b, 1979a, b] included (48) with $\Delta = 0$ in his COTE's (28), keeping β fixed at

$$\beta = 0.10 \quad (50)$$

as originally suggested by Pekeris. This modification eliminated all iteration requirements. Instead of (50), $\beta = 0.08$ and $\beta = 0.12$ were also tested with hardly any different results.

In agreement with all iterative solutions, Accad and Pekeris [1978] and Schwiderski [1978b, 1979a, b] found only moderate modification of the oceanic tide ζ by the ocean loading term ξ . Indeed, hardly any variations in the amplitudes were registered. Some (about 20°) differences in the phases were observed but not always toward improvement of the model. The result is well displayed by Accad and Pekeris [1978, Table 4], where some 1279 empirical tidal data are statistically compared with corresponding values computed with and without ocean loading effects. In particular, for the phases δ ($= t$ in hours) they find the total averages

$$\langle \delta_o - \delta \rangle = 0.9 \quad \langle \delta_o - \delta' \rangle = 0.2 \quad (51)$$

and

$$\langle |\delta_o - \delta| \rangle = 1.0 \quad \langle |\delta_o - \delta'| \rangle = 0.9 \quad (52)$$

where δ_o stands for observed phases and (δ, δ') for computed values without and with ocean loading effects, respectively. The first equations only show that the phase errors seem to be more symmetrically distributed when ocean loading effects are included. The second equations show that there is a meager 10% absolute improvement. The extensive computer experiments of the author clearly demonstrated that there is some improvement with ocean loading effects, which should not (unnecessarily) be neglected. However, considerably more significant improvements (section 5a) were achieved through the inclusion of proper eddy dissipation and bottom friction terms in connection with a hydrodynamically defined ocean basin (sections 3b, 3c, and 4a).

e. Polar Singularities and Ice Caps

In spherical coordinates the COTE's (28) and (29) become singular at the north pole. Most authors avoid this difficulty by terminating the ocean basin at some convenient northern boundary. In order to check his numerical method against an analytic solution in a circular arctic ocean basin, Zahel [1970] derived an analytic integral of the COTE's (28) and (29) without eddy dissipation ($A = 0$). Schwiderski [1978b, 1979a] derived a unique second-order analytic solution of the complete COTE's (28) and (29) which included the special exact integrals discussed in section 2c (equations (24)–(26)). These solutions were matched with the numerical solution (section 4) which started at 4° colatitude southward. Thus all numerical difficulties with the north pole singularities were circumvented, and a more uniform grading of the numerically necessary grid system (section 4a) was achieved.

In all ocean tide models it is tacitly assumed that the polar ice covers have negligible effects on the oceanic tide and currents. This assumption is probably justified within the desired accuracy specified in section 1. It is certainly true at least near the north pole, where, according to section 2c, all semidiurnal and diurnal tides vanish with the second or first power of the distance from the pole. Furthermore, ice cap effects may be introduced indirectly into a tide model by using empirical tide data collected at stations of the Arctic Ocean and at Antarctica in the numerical procedure (section 4c).

4. MODELING DISCRETE OCEAN TIDAL EQUATIONS

a. The Gridded Ocean Basin and Bathymetry

With the advent of electronic computers, hydrodynamical numerical methods dominated the theoretical scene to map worldwide ocean tides. The modern, large-scale numerical investigations were pioneered by Hansen [1948, 1949, 1966], who realized that the complexity of natural ocean basins renders any analytic treatment of the COTE's (28) and (29) intractable. Moreover, as was pointed out by the author (see sections 3a–3c), the COTE's (28) and (29) themselves assume their true physical meaning only in some proper discrete form. Hansen was soon followed by a long line of researchers, such as Gohin [1961], Accad and Pekeris [1963, 1978], Ueno [1964a, b], Bogdanov et al. [1964], Bogdanov and Magarik [1967, 1969], Brettschneider [1967], Tiron et al. [1967], Trepka [1967], Pekeris and Accad [1969], Marchuk et al. [1969, 1973], Zahel [1970, 1973, 1975, 1977], Hendershott [1972, 1975, 1977], Gordyev et al. [1973, 1977], Estes [1975, 1977], Schwiderski, [1976, 1978b, 1979a, b], and Parke and Hendershott [1979].

The definition of a finite-difference analog (DOTE's (60) and (61)) in place of the COTE's (28) and (29) requires a mesh discretization of the ocean area under consideration. While one would like to utilize a grid system as finely detailed as possible to achieve a high resolution of all significant tidal currents, one is, of course, quite limited by the memory capacity of the computer facility available and by the known bathymetric charts of the ocean basin. So far, all grid systems between $6^\circ \times 6^\circ$ and $1^\circ \times 1^\circ$ have been used by numerical tidalists with 'terrestrial' and 'oceanic' mesh cells distinguished by zero or nonzero depth data, respectively. Some authors [e.g., Pekeris and Accad 1969; Parke and Hendershott, 1979; Accad and Pekeris, 1978] terminated the ocean basin at some northern latitude and cast their COTE's into Mercator coordinates. Other analysts [e.g., Zahel, 1970, 1973, 1975, 1977; Estes, 1975, 1977; Schwiderski, 1978b, 1979a, b] retained the entire ocean basin with a grid system that is spherically graded toward the poles, in order to achieve a more uniform mesh area for higher numerical accuracy and stability (section 4b).

For example, the author used a $1^\circ \times 1^\circ$ graded grid system in which each spherically rectangular mesh cell $S_{m,n}$ is bounded by the graded longitudes

$$\lambda_{m-\mu} = (m - \mu)^\circ \quad \lambda_m = m^\circ \quad (53a)$$

and the colatitudes

$$\theta_{n-1} = (n - 1)^\circ \quad \theta_n = n^\circ \quad (53b)$$

where

$$m = \mu, 2\mu, \dots, 360 \quad n = 1, 2, \dots, 168 \quad (54)$$

The 'grading parameter' $\mu = \mu_n$ is defined by

$$\begin{array}{lll} \mu = 1 & n = 30-150 \\ \mu = 2 & n = 15-29 & n = 151-168 \\ \mu = 4 & n = 8-14 \\ \mu = 8 & n = 1-7 \end{array} \quad (55)$$

The grading (equations (55)) was conveniently chosen so that

$$\mu \sin n^\circ \geq \frac{1}{2} \quad n = 4, 8, 15, 30, 150, 165 \quad (56)$$

i.e., the southern mesh size of $S_{m,n}$ remains larger than half the equator mesh size

$$L = \pi R / 180 \approx 111.1775 \text{ km} \quad (57)$$

This important condition is violated for $n = 1^\circ, 2^\circ, 3^\circ, 166^\circ, 167^\circ, 168^\circ$ without reducing the numerical stability of the author's finite difference analog of the COTE's (section 4b). All mesh cells south of colatitude $n = 168^\circ$ are declared antarctic land cells.

The 'mathematically idealized' lateral boundaries of the oceans are generally defined to follow in an obviously zig-zagging fashion the mesh lines of boundary cells. The latter are defined as oceanic cells with at least one neighboring terrestrial cell. Since the ocean boundaries shape the geometry of the tidal currents, the obviously somewhat subjective definition of boundary cells is most significant, especially in models of coarse mesh sizes. After numerous disappointing computations the author found it necessary to distinguish between boundary cells adjacent to continental and island land masses. In agreement with *Smith et al.* [1966], grid cells near continents were declared oceanic boundary cells if at least half of their mesh areas contained a water depth of more than 5 m; otherwise those cells were designated terrestrial cells. The same principle was applied to grid cells near islands large in area. However, grid cells crossed by elongated islands or island chains were declared terrestrial cells even if the island area was small in comparison to half the mesh area. Although a $1^\circ \times 1^\circ$ grid system was used, the latter condition was found to be necessary in order to retain the hydrodynamically important separation properties of elongated islands and island chains. Remaining oceanic cells that were gridwise disconnected from the main oceans (e.g., the entire Mediterranean Sea) were redefined as terrestrial cells.

The artificial zigzagging boundary of the ocean basin caused some instability or resonance problems in the numerical procedures of some researchers [e.g., *Pekeris and Accad*, 1969; *Parke and Hendershott*, 1979; *Accad and Pekeris*, 1978] using nondissipative COTE's ((28) with $A = B = 0$). In order to overcome these difficulties, smoothed boundaries and depth data were artificially introduced. No such difficulties were reported by analysts using dissipative COTE's. The author's computer experiments with the full COTE's (28) and (29) displayed no discernible differences for rough or smoothed boundaries.

For the worldwide oceans, essentially $1^\circ \times 1^\circ$ averaged depth data were compiled by *Dishon* [1964] and *Dishon and Heezen* [1968] and independently by *Smith et al.* [1966]. The latter collection has been somewhat revised by *Gates and Nelson* [1975], and both sets are available in tape form. In spite of specially collected depth data, all investigators prepared their own bathymetric charts corresponding to the grid system chosen. Those data were quite drastically curtailed by artificial limits on both the shallow and the deep ends of the depth range. Moreover, the stability requirements of the numerical

schemes, especially in the dissipationless case, forced some numerical analysts [e.g., *Pekeris and Accad*, 1969; *Parke and Hendershott*, 1979; *Accad and Pekeris*, 1978] to apply drastic smoothing operations to the bathymetric data used.

Obviously, in such an ocean geometry, much of the absolutely necessary resolution of, say, narrow ocean ridges and continental shelves is lost. In fact, the corresponding computed tidal maps (see the collections by *Hendershott* [1973, 1977] and *Parke* [1978]) suffer most of all from the lack of proper resolution of bottom and boundary (see discussion above) irregularities. One may expect a $1^\circ \times 1^\circ$ seamount or island to have little effect on the surrounding tidal wave, but a row of such obstacles over several mesh cells represents a hydrodynamical barrier separating the tidal currents on both of its sides.

In exploratory computations, *Schwiderski* [1978b, 1979a, b] used the dissipative COTE's (28) and (29) with the rough gridwise adjusted depth data of *Smith et al.* [1966] and detected no instabilities in the numerical method. However, although the preliminary tidal model [*Schwiderski*, 1976] satisfied some accuracy requirements in tidal applications [e.g., *Goad and Douglas*, 1977a, b], the model still failed to resolve the well-known (see sections 2b and 5a) large tidal deformations and retardations over narrow ocean ridges (e.g., Aleutian, Hawaiian, and Caribbean) and continental shelves. This experience led to a redefinition of the *Smith et al.* [1966] depth data in over 3000 grid cells on the basis of the following hydrodynamical principles in connection with the definition of oceanic and terrestrial cells given above [*Schwiderski*, 1978a].

1. In oceanic boundary cells near continents or large islands the averaged oceanic depth was assigned as the mean depth of the entire grid cell.

2. In oceanic cells crossed by shallow submerged or partly submerged ridges the average ridge depth was assigned as the mean depth of the whole grid cell.

It may be noted that the 'hydrodynamically defined' depth (1) replaces the 'statically defined' depth of *Smith et al.* [1966], which preserves the estimated water mass of the boundary cell and thus may introduce an artificial shelflike character to the cell. Exploratory computations with the new ocean bottom relief in connection with the novel depth-dependent eddy viscosity (30) and depth-independent bottom friction coefficient (41) dramatically reflected the improved resolution. The improvement of the tide model was even more spectacular when empirical tidal data were hydrodynamically interpolated (section 4c and 5a). Naturally, it must be kept in mind that the definition of depth values, in particular in boundary cells, is (even with the knowledge of numerous soundings) quite subjective and hence subject to some error. However, isolated inaccuracies of this sort were generally found ineffective in altering the overall quality of the tidal model.

b. Discrete Ocean Tidal Equations

On the gridded ocean basin (section 4a) the differential equations of oceanic tidal motions (COTE's (28) and (29)) can be converted into physically meaningful discrete finite difference equations for a computerized solution. Since the beginning of the computer age, numerous finite-differencing schemes with various characteristics have been developed and tested by numerical analysts working in applied mathematics, fluid mechanics, oceanography, and meteorology. The application of these techniques with or without possible variations to the present COTE's depends essentially on the numerical

Fig.
staggered
circles

tidalist
limited

Foll
deriva
placed
system
the dif
stagge
variab
cated,
Figure

If on
as the
tegrated
value
compl
provid
ties (e
model
these
genera
may b
ampli
is dire
ity eq
bound
pliicit
by me
dissip
solved
verte
cad [1

In
eddy
ence
differe
(21) a
obviou
data
matic
simpl
such
1969]
[1979]

Sim
integrat
and s
ocean
most
realisti
linear
3c) a
tion
(e.g.,

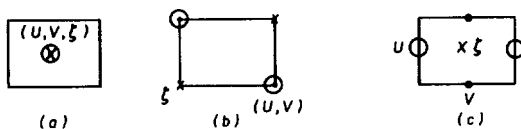


Fig. 5. Finite-difference schemes in space: (a) regular, (b) semi-staggered, and (c) (fully) staggered. Open circles are U points, solid circles are V points, and crosses are ξ points.

tidalist's empirically founded modeling skill and imagination, limited only by the available computer capacity.

Following the usual procedure, in the first step, all spacial derivatives in the COTE's (28), (29), (33), and (37) may be replaced by central finite differences corresponding to the grid system chosen. As was first pointed out by Richardson [1922], the differencing scheme may be chosen to be 'regular,' 'semi-staggered,' or (fully) 'staggered'; that is, the three dependent variables (U , V , ξ) may be computed and tabulated at collocated, semidislocated, or fully dislocated points, as shown in Figure 5.

If only a partial equilibrium tide η (section 2a) is considered as the driving force, the remaining equations may be integrated as a boundary value problem (BVP) or as an initial value problem (IVP). In the BVP approach one removes the complex time periodic factor by the substitution given in (20), provided the COTE's are strictly linear. (If nonlinear properties (e.g., square law of bottom friction (equation (39))) are modeled, infinite Fourier series could in principle be used, but these lead to an involved infinite system of equations.) In the general case (GBVP) the resulting three difference equations may be combined into two equations for the complex velocity amplitudes by eliminating the complex tidal amplitude, which is directly computable from the velocity field via the continuity equation (compare (21) and (22)). With sufficient velocity boundary conditions (section 4c) one winds up with an implicit complex system of linear equations that can be solved by modern computerized methods. If the higher-order eddy dissipation terms of (33) are included, the linear system to be solved is drastically simplified and has been successfully inverted by Accad and Pekeris [1963, 1978] and Pekeris and Accad [1969].

In the special boundary value problem (SBVP), where all eddy dissipation terms are neglected, the same three difference equations derived above can be combined into a single difference equation for the complex tidal amplitude (compare (21) and (22)). This alternative approach to the linear BVP is obviously advantageous whenever empirical tidal boundary data (section 4c) are introduced in place of the purely mathematical velocity boundary data required in the GBVP. The simple SBVP attracted the attention of several investigators, such as Hansen [1948, 1949], Bagdanov and Magarik [1967, 1969], Hendershott [1972, 1975], and Parke and Hendershott [1979], who also neglected bottom friction.

Since the basic tide model is time dependent, it may be integrated as an IVP starting from some arbitrary initial state and so offer itself as an experimental field for more involved oceanic or atmospheric circulation studies. In addition, this most natural approach leaves unrestricted room for full-scale realistic modeling of tidal currents, including linear or non-linear eddy dissipation and bottom friction (sections 3b and 3c) as well as mathematical or empirical boundary data (section 4c). In fact, the resulting discrete ocean tidal equations (e.g., DOTE's (60) and (61)) permit a relatively easy examina-

tion (see discussion below) of the physically important decay and dispersion features of the oceanic motions modeled.

In the IVP approach, the first-order time derivatives of the COTE's (28), (29), (33), and (37), in which all spacial derivatives have been replaced by some finite-difference scheme (see discussion above), may be inverted by integration over one or two time steps Δt along the degenerated characteristic of the system i.e., parallel to the t axis. (It may be suggested here that an integration along the ruled lines of the characteristic cone of the system might be preferable, but this alternative has never been tried in modeling of ocean currents.) The remaining (not explicitly integrable) integrals are then replaced by some average (one, two, or three point) integration rule such as

$$\int_{t_j}^{t_{j+1}} U(t) dt = \Delta t [\kappa U^{j+1} + (1 - \kappa) U^j] \quad (58)$$

where κ ($0 \leq \kappa \leq 1$) denotes some 'difference parameter' and

$$U^j = U(t_j) \quad t_j = (j - 1)\Delta t \quad j = 1, 2, \dots \quad (59)$$

Depending on the chosen time integration formula, the obtained DOTE's must be solved either by an explicit or by an implicit time-stepping procedure that begins with some initial state. As was recognized by Richardson [1922], the time integration may utilize a regular, a step-over (or leapfrog), or an intermediary (or alternating) time-stepping scheme. In the regular scheme, all three (real) variables (U , V , ξ) are computed and tabulated at the same time points (Figure 6a). In Richardson's step-over (now often called leapfrog) method, both velocity components (U , V) are cotimed, but the tidal elevations ξ are computed and tabulated at intermediate time points (Figure 6b). In the intermediary (or alternating) procedure, all three variables (U , V , ξ) are computed and tabulated coincidently; however, both velocity components use computationally auxiliary intermediate time points in an alternating fashion (Figure 6c).

Although the step-over scheme is widely used in general ocean current and atmospheric circulation studies, the regular and intermediary schemes seem to have been preferred in tidal models. The intermediary method has been applied in a rather involved explicit-implicit form by Marchuk *et al.* [1969, 1973] and Gordeyev *et al.* [1973] to tidal computations in border seas and in a global ocean model. In the now well-known 'hydrodynamical-numerical' method of Hansen [1966] the staggered scheme in space is combined with the regular scheme in time in an explicit and convenient fashion. This method was successfully applied by Zahel [1970, 1973, 1975, 1977] and Estes [1975, 1977] and in a modified version by the author [Schwiderski, 1978b, 1979a, b].

By applying the integration rule of (58), using $\kappa = 0$ and $\kappa = 1$ in the momentum equations and $\kappa = 1$ in the continuity equation, one arrives at the following explicit, regular,

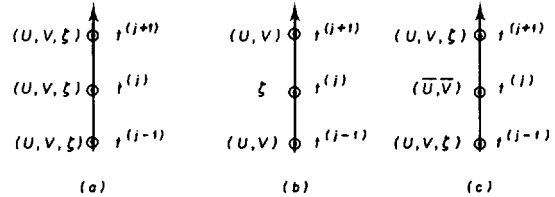


Fig. 6. Finite-difference schemes in time: (a) regular, (b) step over (leapfrog), (c) intermediary (alternating); (U , V , ξ) are computed and tabulated, (\bar{U} , \bar{V}) are computed but not tabulated.

and staggered DOTE's corresponding to the COTE's (28), (29), (33), and (37) and the grid system defined by (53).

$$\begin{aligned} [1 + \kappa A_{m,n}^4] U_{m,n}^{j+1} &= A_{m,n}^{-1} \sin(\sigma\Delta t/2)(2j-1) \\ &+ A_{m,n}^{-2} \cos(\sigma\Delta t/2)(2j-1) \\ &+ A_{m,n}^{-3} [\zeta_{m-\mu,n} - \zeta_{m,n}] + [1 - (1 - \kappa) A_{m,n}^{-4}] U_{m,n}^{-1} \\ &+ A_{m,n}^{-5} U_{m+\mu,n}^{-1} + A_{m,n}^{-6} U_{m-\mu,n}^{-1} + A_{m,n}^{-7} U_{m,n+1}^{-1} + A_{m,n}^{-8} U_{m,n-1}^{-1} \\ &+ A_{m,n}^{-9} [V_{m,n}^{-1} + V_{m,n-1}^{-1}] - (V_{m-\mu,n}^{-1} + V_{m-\mu,n-1}^{-1}) \\ &+ A_{m,n}^{-10} [(V_{m,n}^{-1} + V_{m,n-1}^{-1}) + (V_{m-\mu,n}^{-1} + V_{m-\mu,n-1}^{-1})] \end{aligned} \quad (60a)$$

$$\begin{aligned} [1 + \kappa B_{m,n}^4] V_{m,n}^{j+1} &= B_{m,n}^{-1} \cos(\sigma\Delta t/2)(2j-1) \\ &+ B_{m,n}^{-2} \sin(\sigma\Delta t/2)(2j-1) \\ &+ B_{m,n}^{-3} [\zeta_{m,n+1} - \zeta_{m,n}] + [1 - (1 - \kappa) B_{m,n}^{-4}] V_{m,n}^{-1} \\ &+ B_{m,n}^{-5} [V_{m+\mu,n}^{-1} + V_{m-\mu,n}^{-1}] + B_{m,n}^{-6} V_{m,n+1}^{-1} + B_{m,n}^{-7} V_{m,n-1}^{-1} \\ &+ B_{m,n}^{-8} [U_{m+\mu,n+1}^{-1} - U_{m,n}^{-1}] + B_{m,n}^{-9} [U_{m+\mu,n}^{-1} - U_{m,n+1}^{-1}] \\ &+ B_{m,n}^{-10} [U_{m+\mu,n+1}^{-1} + U_{m,n}^{-1} + U_{m+\mu,n}^{-1} + U_{m,n+1}^{-1}] \end{aligned} \quad (60b)$$

$$\begin{aligned} \zeta_{m,n}^{j+1} &= \zeta_{m,n}^{-1} + [C_n^{-1} (U_{m,n}^{j+1} - U_{m+\mu,n}^{j+1}) \\ &+ C_n^{-2} V_{m,n}^{j+1} - C_n^{-3} V_{m,n-1}^{j+1}] \end{aligned} \quad (61)$$

Following standard principles [e.g., *Richtmyer and Morton*, 1967], *Zahel* [1970] and *Schwiderski* [1978b, 1979a] showed that the DOTE's (60) and (61) with 'locally constant' coefficients yield Fourier-type eigensolutions of the form

$$\begin{aligned} U_{m,n}^{-j} &= U_0 d^j \exp[i(\gamma_1(2m-2\mu)\Delta\lambda + \gamma_2(2n-1)\Delta\theta)] \\ V_{m,n}^{-j} &= V_0 d^j \exp[i(\gamma_1(2m-\mu)\Delta\lambda + \gamma_2 n \Delta\theta)] \quad (62) \\ \zeta_{m,n}^{-j} &= \zeta_0 d^j \exp[i(\gamma_1(2m-\mu)\Delta\lambda + \gamma_2(2n-1)\Delta\theta)] \end{aligned}$$

with an arbitrary wave vector (γ_1, γ_2) and some nonzero amplitude vector (U_0, V_0, ζ_0), provided d satisfies a cubic eigenvalue equation. Obviously, the DOTE's will be stable if the three eigenvalues (d_0, d_1, d_2) fulfill at all oceanic points the 'stability condition'

$$|d_k| \leq 1 \quad k = 0, 1, 2 \quad (63)$$

This requirement, which was found to be scrupulously binding, can be met by restricting the reduced eddy viscosity a (in (30)), the mesh length L , the time step Δt , and the differencing parameter κ to appropriate stability ranges. Within those ranges these parameters and the always stabilizing bottom friction coefficient b (in (41)) remain free to be determined by trial-and-error computations to achieve optimum results.

For a stationary earth ($\Omega = 0$) and zero bottom friction the author found d_0 to be real and positive. Hence the corresponding eigenwave (equations (62)) represents a standing but decaying wave with no phase shift. Under an additional condition imposed on the free parameters mentioned above, the other eigenvalues d_1 and d_2 became conjugate complex and defined a pair of eigenwaves progressing in opposite directions with the same decay and dispersion rates.

It is interesting to note that for a $1^\circ \times 1^\circ$ grid system and sufficiently small time steps Δt (about 3 min) the amount of eddy dissipation was only limited from above and not at all from below. Hence the actual magnitude of the eddy viscosity (A in (32)) was solely determined by the quality of the computed tidal model and not by some artificial mathematical shortcoming. Furthermore, the rate of decay of all eigenwaves

(equations (62)) was found to be directly dependent on the eddy viscosity $A = \bar{a}H$ (equation (30)). Thus for a fixed \bar{a} , waves in deep ocean basins decay faster than those in shallow regions if bottom friction is neglected. It was this physically realistic feature that led to the introduction of the novel depth-dependent eddy viscosity. For a constant A , waves would decay at the same rate in deep or shallow oceans even though no bottom friction were present. This latter situation is physically unacceptable in an ocean of strongly varying bathymetry and produced, indeed, unrealistic results.

At this point, attention of the more mathematically oriented reader should be drawn to the extensive and important investigations of *Marchuk et al.* [1969, 1973], *Gordeyev et al.* [1973, 1977], *Kagan* [1977], and *Marchuk and Kagan* [1977]. These authors used powerful modern methods of functional analysis to prove rigorously the stability and convergence properties of their unique finite-differencing schemes. A detailed analysis of these techniques exceeds, however, the scope of this review.

c. Lateral Empirical and Mathematical Boundary Data

In order to specify a unique integral of the ocean tidal equations in continuous or discrete form, proper lateral boundary data must be imposed. Attracted by the simplicity of the special boundary value problem (section 4b), which is reduced to a single equation for the complex tidal amplitude, *Hansen* [1948, 1949] supported his early tide models with empirical tidal boundary data known around the ocean basin considered. Although the SBVP has been applied by several investigators, it is restricted to lateral dissipationless linear models and leaves the fluid flow across the ocean boundaries without any control (compare hydrodynamical interpolation below). Such an unchecked violation of the 'stiff' condition of conservation of mass is obviously somewhat hazardous. For example, it played probably a major role in *Hendershott's* [1975] divergent iteration attempt to include ocean-loading effects in his tide model (see section 3d and *Farrell* [1972b]). In fact, the convergent *Accad and Pekeris* [1978] tide model differs from the Hendershott model only in the imposed boundary conditions, where the former (equation (64)) places some indirect control on the allowed violation of conservation of mass.

Instead of empirical boundary values, *Accad and Pekeris* [1963] introduced the mathematical boundary condition of 'no flow' across the ocean shorelines, which is sufficient to specify a unique solution of their GBVP (section 4b) without lateral eddy dissipation. However, when higher-order eddy dissipation terms are included in the GBVP or in the complete IVP, two sets of boundary data are required to determine a unique integral. *Hansen* [1966], *Zahel* [1970, 1972, 1975, 1977], *Estes* [1975, 1977], and others used the complete mathematical boundary conditions of no flow across and 'free slip' along the ocean boundaries. Some authors [e.g., *Marchuk et al.*, 1969] replaced the free-slip condition by the 'no slip' condition, which is appropriately used to specify laminar flows. In turbulent flows with very thin boundary layers and large eddy viscosities the free-slip condition is generally preferred and is more consistent with all other simplifications of the tidal model (section 3a). The author's computer experiments with both the free-slip and the no-slip conditions exhibited only a slight preference for the first one.

Some numerical tidalists used a mixture of tidal and velocity boundary conditions. For example, *Tiron et al.* [1967] used

empirical
the cond
Accad a
[1952] a
relations

where u
paramet
that neg
along th
shelf po
able pre
and on t
ties we
It may b
the exact
appears
cause it
depth H

The a
with the
strated e
and reta
section 2
factorily
direct in
dynam
incorp
lected (s
anic bo
such as
this me
IVP's w
the auth
Hansen

Assu
tidal am
ical val

replaces
the con
computo
no-flow
the subs
nuity ga

that sig
conserv
above).

The
direct c
(equatio
the spe
slope an
mented
(61) b
gap as
techniq
ficient b
the cent

on the fixed \bar{a} , shallow physically the novel waves even equation is bying ba... oriented inves...l. [1973,]. These analysis properties of analysis of review.

mean tidal or lateral implicity which is amplitude, with em...an basin by several less linear boundaries interpolation condition of elous. For dershott's ading ef...[1972b]). In model dif...d bound...aces some vation of

d Pekeris dition of ficient to) without der eddy complete determine a 72, 1975, te mathe... 'free slip' archuk et slip' con... flows. In large eddy red and is the tidal enents with ed only a and veloc...967] used

empirical tidal elevations wherever they were available and the condition of no flow across the coastline everywhere else. Accad and Pekeris [1978] generalized an idea of Proudman [1952] and introduced a mixed mathematical tide-velocity relationship of the form

$$\zeta = ru_N \quad (64)$$

where u_N denotes the velocity normal to the boundary. The parameter r was derived for a simple sloping shelf wave model that neglects any contribution from the tangential motion along the shoreline and specifies no breadth of the horizontal shelf portion. The value of r was found to depend on the variable preshelf ocean depth H , on the horizontal shelf depth H' , and on the width of the shelf slope S , where the last two quantities were arbitrarily fixed at $H' = 10$ m and $S = 0$, or 100 km. It may be noted that this boundary condition does not fulfill the exact continuity equation (equation (29) or (61)). Also, it appears only formally as a purely mathematical condition, because it depends directly on the assigned ocean boundary depth H , which is largely subjective (section 4a).

The author's [Schwiderski, 1978b, 1979a, b] experiments with the no-flow and free-slip boundary conditions demonstrated convincingly that the important localized distortions and retardations of tides at shore or bottom irregularities (see section 2b, Figure 3, and Tables 4a and 4b) could not be satisfactorily modeled on a $1^\circ \times 1^\circ$ grid system without a proper direct inclusion of empirical tidal data. A unique 'hydrodynamical interpolation' technique was developed that incorporates into the tide model over 2000 empirical data selected (see discussion below) as being representative for oceanic boundary cells and oceanic cells with bottom anomalies such as small islands, seamounts, or coastal banks. Though this method is in principle applicable to all GBVP's and IVP's with bottom friction, it is technically most adapted to the author's modified version ($\kappa = 1$ in the DOTE's (60)) of Hansen's hydrodynamical-numerical difference scheme.

Assuming that for the oceanic grid cell $S_{m,n}$ the empirical tidal amplitude $\xi_{m,n}$ and phase $\delta_{m,n}$ are known, then the empirical value

$$\xi_{m,n}^{j+1} = \xi_{m,n} \cos(\sigma\Delta t j - \delta_{m,n}) \quad (65)$$

replaces the corresponding mathematical value determined by the continuity equation (61), where the velocity entries are computed earlier by using the DOTE's (60) with $\kappa = 1$ and the no-flow and free-slip conditions for boundary cells. Of course, the substitution of (65) for the DOTE (61) constitutes a 'continuity gap'

$$\Delta\xi_{m,n}^{j+1} = \xi_{m,n}^{j+1} - \xi_{m,n}^j \quad (66)$$

that signals a periodic violation of the sensitive condition of conservation of mass which must be checked (see discussion above).

The continuity gap was significantly narrowed by an indirect cellwise adjustment of the bottom friction coefficient b (equation (41)), which depends on the physical properties of the special cells considered, such as true cell size and bottom slope and roughness. The indirect adjustment of b was implemented by simply modifying the velocity entries in the DOTE (61) by using bounded multipliers that closed the continuity gap as much as possible while yielding optimum results. This technique is justified, since for $\kappa = 1$ the bottom friction coefficient b appears only on the left sides of the DOTE's (60) in the central coefficients $A_{m,n}^{-4}$ and $B_{m,n}^{-4}$, which additionally in-

clude only negligible depth-dependent eddy dissipation effects (equation (30)). By trial and error, best results were obtained when the uniform coefficient $b = 0.01$ m/s was allowed to vary to a maximum of $b = 0.04$ m/s. It must be mentioned that no physical justification was found to apply the same bottom friction adjustment technique to distant offshore oceanic cells with available deep-sea tide measurements (see Table 3).

In order to narrow further the continuity gaps in oceanic boundary cells the mathematically defined land-ocean boundary lines (section 4a) were implicitly replaced by more realistic shorelines. This redefinition was accomplished by allowing over the mathematical boundary segments limited periodic inflows or outflows (Figure 7) that reduced the continuity gaps to acceptable levels. In general, the continuity gaps (equation (66)) dropped significantly below half the corresponding empirical elevation change during the same time step Δt . The remaining uniformly moderate continuity gaps and velocity distortions could then be attributed to other physical inaccuracies of the tide model, such as faulty depth data (section 4a) erratic empirical tide data (see discussion below), and neglected nonlinear effects (sections 3a and 3c).

The novel hydrodynamical interpolation technique, which is described in full detail by Schwiderski [1978b, 1979b], has been tested and evaluated for its important smoothness characteristics, which are distinctly different from other direct (e.g., polynomial) interpolation methods. The adjustment of hydrodynamical parameters does not imply any smoothness of the interpolation, unless both the empirical data and the hydrodynamical model are compatible with each other. As can be seen in Figure 3 and in Tables 2, 4a, and 4b, it is an important exclusive feature of the hydrodynamical interpolation that it preserves the physically realistic (i.e., observed) roughness of ocean tides near uneven shorelines, islands, and oceanic ridges.

Some objections against the use of certain unreliable empirical tide data have been raised by tidalists who experienced difficulties in selecting meaningful tidal boundary data from the available collections. As was pointed out in section 2b, the same criticism applies to some degree to all empirical tide data, none of which are exact measurements; all are mathematically treated by more or less subjective and controversial methods. Nevertheless, the bulk of the listed data were found to be sufficiently accurate for the corresponding stations and their immediate neighborhoods. The problem of choice (which resembles the selection of bathymetric boundary data (section 4a)) is certainly not overcome by excluding empirical tide data from the model but afterwards judging the modeled data against such unreliable values.

The crux of the matter is to select from the massive listings data that are representative for the corresponding oceanic cells. Although empirical tide data have been used for some time in direct or indirect applications to modeling of ocean tides, only Zahel [1970, 1973] and Schwiderski [1978b, and 1979b, c] published the complete sets of selected data. The author described also the detailed selection process involved. In principle, the collected data were subjected to an initial screening in order to eliminate obviously erratic and sheltered-station data. Out of the still remaining mass of sometimes rough and seemingly incoherent tidal constants, 'representative' data were determined by taking averages over the mesh area with weights biased toward more ocean exposures and more coherent relationships with values of adjacent cells. The application of such averaging principles is apparently

TABLE 3. Deep-Sea M_2 Tide Data for the Pacific, Atlantic, Mexican Gulf, and Caribbean Sea

Station	Geographic Coordinates		Observation		Model*		Error	
	°N	°W	ξ , cm	δ , deg	ξ , cm	σ , deg	$\Delta\xi$, cm	$\Delta\sigma$, deg
<i>Pacific</i>								
Middleton (1)	58.76	145.71	110	284				
Tofino (3)	48.97	127.29	99	239				
San Francisco	38.16	124.91	54	227				
Josie II	34.00	144.99	27	267	27	273	0	+6
Flicki	32.24	120.86	43	149				
Josie I	31.03	119.80	43	142				
Kathy	27.75	124.37	29	128	27	130	-2	+2
Filloux	24.78	129.02	19	107	18	105	-1	-2
<i>Atlantic</i>								
N.Y. Bight	39.32	64.36	44	350				
N.C. 1	32.69	75.62	48	356	46	358	-2	+2
Savannah B	31.95	80.68	88	15				
Scope	30.43	76.42	45	358	46	3	+2	+5
AOML 1	28.14	69.75	34	1	35	6	+1	+5
AOML 3	28.24	67.54	34	359	34	4	0	+5
MERT	27.99	69.67	34	360	34	6	0	+6
REIKO	27.97	69.67	35	1	34	6	-1	+5
EDIE-May	26.46	69.33	32	3	32	7	0	+4
EDIE-March	26.45	69.32	31	1	32	7	+1	+6
<i>Mexican Gulf</i>								
West Florida Shelf	26.71	84.25	7	97	7	92	0	-5
Deep Gulf	24.77	89.65	1.3	226	1.6	225	+0.3	-1
<i>Caribbean</i>								
Misteriosa Bank	18.88	83.81	8	84	9	89	+1	+5
Rosalind Bank	16.61	80.34	7	107	8	102	+1	-5
East Caribbean (6 month)	16.54	64.88	0.5	156	1.6	151	+1	-5
East Caribbean (1 month)	16.52	64.91	0.6	153	1.5	148	0.9	-5

Here ξ is the tidal amplitude and δ is the tidal phase relative to Greenwich

*Where there is no entry, ξ and δ are included.

consistent with the definition of mean turbulent tidal velocities and elevations given in section 3a, which, incidentally, is directly suggested by the discrete continuity equation (61). Indeed, the excess of fluid flux into a grid cell during a time interval Δt divided by the mesh area produces the increase $\Delta\xi$ in the average tidal height ξ .

For example, the author determined from the various tidal constants listed in Table 2 for stations near Bermuda the values $\xi = 37$ cm and $\delta = 0^\circ$ shown in Tables 4a and 4b for the $1^\circ \times 1^\circ$ oceanic cell (BI) containing the small island of Bermuda. Of course, in areas of extremely rough tides the averaging process was much more critical. Nevertheless, such uncorrelated data must be considered as being indicative of intensely turbulent or eddying tidal motions produced by the open ocean currents on shallow shelves, for example, in front of rivers or coastal corners (section 2b). Vice versa, the open ocean tides must be modeled to be flexible enough in order to accept rough empirical data with only moderate and localized backslash effects on themselves. As is shown in Figure 3 and in Tables 4a and 4b, the hydrodynamical interpolation technique described above meets this requirement to a satisfactory degree. In fact, perturbations were tested that were caused by deliberately created large 'errors' in 'empirical' amplitudes and phases of isolated cells. The computations remained stable, and only minor localized alterations were registered as if they were caused by a sudden birth of a volcanic island.

Naturally, in any selection the representative empirical tide data are strongly mesh size dependent and may become meaningless in very coarse grid systems. For instance, a $6^\circ \times 6^\circ$ network covers the breadth of the Atlantic between Brazil and North Africa with only four cells, and two of them are

supposed to carry empirical data. In such a grid system the resolution of the entire Atlantic width is about the same as the resolution of, say, the Davis Strait in a graded $1^\circ \times 1^\circ$ network. Moreover, in contrast to coarser grid systems a $1^\circ \times 1^\circ$ network allows for a clear differentiation between shallow and deep ocean waves. As the momentum equations (28) show, tidal slopes in deep and shallow oceanic cells are multiplied by the corresponding ocean depths of, say, $H = 5000$ m and $H = 50$ m. Hence small tidal variations in deep oceans appear to be more significant than, say, tenfold larger tidal slopes in shallow areas, which explains the observed (see discussion above) insensitivity of the open ocean tide with respect to locally large tidal boundary data.

5. DISCUSSION OF OCEAN TIDAL MODELS

a. Evaluation of Ocean Tidal Charts

Recent ocean tidal maps, which have been charted by various empirical and theoretical methods, are qualitatively compared and discussed in the review articles by Hendershott [1973, 1977] and Parke [1978]. Of course, every author discussed the quality of his own tide model by comparing it with earlier charts and with some empirical tide data either pointwise or statistically. Hence it suffices here to summarize the major characteristics of ocean tides and to describe briefly a new approach to graphical evaluation of the detailed numerical accuracy of a tidal chart.

In order to display the qualitative global features of open ocean tides the author's constructed M_2 tide is plotted in the usual map form in Figure 8. As was anticipated in section 2c, one finds the crests of the tidal waves rotating around amph-

dromic points of zero amplitudes. Although this general feature has been known for some time, the number and the detailed distribution of these amphidromic systems varied from model to model and caused considerable controversies. However, as was pointed out by Parke [1978], the recent models have reached a considerable degree of similarity, and many of the remaining differences emerged as being theoretically insignificant. Indeed, several seemingly major amphidromic systems that were displayed by some maps but failed to show up on other charts are now resolved by the author's model as double amphidromes or as low-amplitude tides.

For example, Pekeris and Accad [1969] discovered an amphidromic system in the north central South Atlantic (see Figure 8), which motivated Cartwright's [1971] tidal measurements around Saint Helena that produced no definitive decision. The same amphidrome appeared later in slightly different positions in the model of Zahel [1970, 1977], Gordyev et al. [1973], Estes [1975, 1977], Schwiderski [1976], and Accad and Pekeris [1978]. Earlier empirical and theoretical maps, as well as the Hendershott [1972] chart, failed to resolve this system completely. As was noticed by Parke [1978], the author's (Figure 8) new model resolves this controversy by a double amphidromic system, which settles in between the two opposing results and is qualitatively close to the low-amplitude tide found in the Parke and Hendershott [1979] chart. Similar situations can be identified, for example, in the Indian Ocean south of Australia, in the Pacific between the Marianas and Marshall Islands, and also near the Hawaiian Ridge. The last case played an important role in the development of the author's tide model, which has been fully discussed by Schwiderski [1978b, 1979b].

The display of ocean tides by maps of the form shown in Figure 8 is obviously inadequate to permit a thorough grid-wise accuracy evaluation as specified in sections 1 and 2b. In order to eliminate these shortcomings, Schwiderski [1978b, 1979b] adopted a new method to display ocean tides graphically by computerized printing of all gridded amplitudes and phases in maplike tables. For example, Tables 4a and 4b exhibit vividly all the detailed features of the M_2 tide in the $30^\circ \times 50^\circ$ area of the northwestern Atlantic Ocean, which the author's model has actually resolved. A brief glance at these tables reveals that the corresponding portion of Figure 8 leaves all tidal features in this important area either unreproduced or completely blurred. It seems that for this reason, Parke [1978] suppressed most of these deficiencies in his reproduction of Figure 8.

In addition to the computed data the tidal Tables 4a and 4b depict also by special markings all empirical coastal and island data (subbars) and nearshore deep-sea data (subbrackets) that were included in the computations. Computed data near distant offshore deep-sea tide stations are marked by wavy underlines to be readily available for comparison with the corresponding empirical deep-sea data listed in Table 3. As can be seen in Table 3, the maximum amplitude and phase differences (possibly error estimates) between the empirical deep-sea data and the computed data are $\Delta\xi = 2$ cm and $\Delta\delta = 6^\circ \approx 12$ min. At the Atlantic Scope station the tide prediction differences in the sense of (10) and (12) are $\xi_m = 4.1$ cm and $E = 2.9$ cm. These minor differences are probably within the empirical error due to short observation times and the use of the distant shore reference station Bermuda [Zetler et al., 1975]. As is shown in Table 2, the various empirical tidal constants for shore and nearshore stations at Bermuda

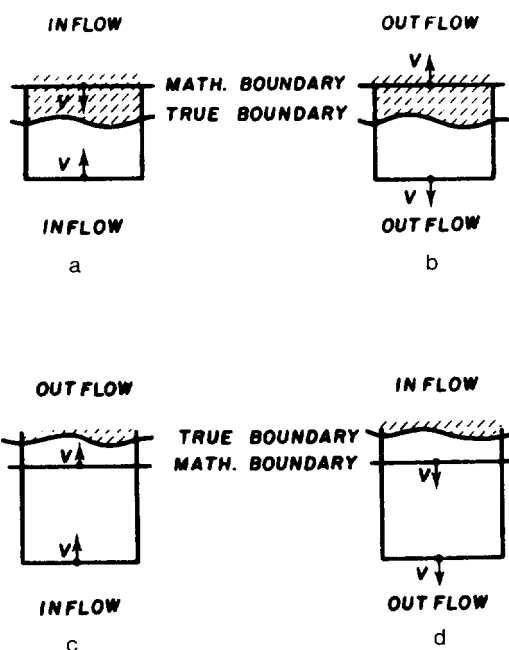


Fig. 7. Boundary cell inflow and outflow illustration. Figures 7a and 7b and Figures 7c and 7d are half periods apart. (The shaded regions are land areas.)

differ by 4 cm in amplitudes and $16^\circ \approx 32$ min in phases. In this connection, attention may be drawn to the differences between the empirical deep-sea data determined by Kuo and his co-worker Malone without and with filter techniques for the nearby GOBI stations.

Since the phases specify the arrival times (in $1^\circ \approx 2$ min (section 2a) of the tidal crests at the corresponding points after the moon's passage over Greenwich meridian, one can easily follow the motion of the tidal waves in Table 4b by starting, say, at the prominently visible $0^\circ = 360^\circ$ (or 100°) cotidal lines. Table 4a lists the corresponding water heights of the crests. Thus using both tables together, one gathers a vivid impression of the motion of tidal waves and their interactions with each other and with empirical data to which they must adjust themselves in a physically flexible way (see section 4c). In particular, one can see the tidal crests producing high and rough waters along uneven coastlines (e.g., between Cape Cod and Nova Scotia). An impressive reproduction of this recently empirically verified feature is depicted in Figure 3.

In the southern portion of Table 4b one can follow the tidal crest from the 0° cotidal line on its semidiurnal complete rotation around the amphidromic point (marked by a circled cross) in the Caribbean Sea southeast of the island of Puerto Rico (PRI). There along the Caribbean Ridge, one recognizes the remarkable resolution of the empirically long-known (section 2b) distortions and retardations which tidal waves suffer as they spill over narrow ocean ridges. As is described by Schwiderski [1978b, 1979b], the close reproduction of this important phenomenon along the Marianas, Nampo, Kuril, Aleutian, and Hawaiian ridges, which almost separate the tides in the Pacific from those in the Philippine, Okhotsk, and Bering seas, brought about a spectacular turnaround of the north central Pacific M_2 tide affecting the whole Pacific Ocean.

By extending the same detailed scrutiny outlined above to the entire constructed global M_2 tide, Schwiderski [1978b,

TABLE 4a. M_2 Tidal Amplitudes ξ (in Centimeters) of the Northwestern Atlantic Ocean

TABLE 4b. *M.* Tidal Phases (in Degrees) of the Northwestern Atlantic Ocean

TABLE 4b. M_2 Tidal Phases δ (in Degrees) of the Northwestern Atlantic Ocean

N	280	281	282	283	284	285	286	287	288	289	290	291	292	293	294	295	296	297	298	299	300	301	302	303	304	305	306	307	308	309	
32																															
33																															
34																															
35																															
36																															
37																															
38																															
39																															
40																															
41																															
42																															
43																															
44																															
45																															
46																															
47																															
48																															
49																															
50																															
51																															
52																															
53																															
54																															
55																															
56																															
57																															
58																															
59																															
60																															
61																															
62																															
63																															
64																															
65																															
66																															
67																															
68																															
69																															
70																															
71																															
72																															
73																															
74																															
75																															
76																															
77																															
78																															
79																															
80																															
81																															

M is longitude east (in degrees), N is the colatitude (in degrees), circled crosses are amphidromic points, subbars mark empirical input data, subbrackets mark input nearshore deep-sea measurements, and wavy underlines mark offshore deep-sea tide gauge stations with excluded measurements listed in Table 3.

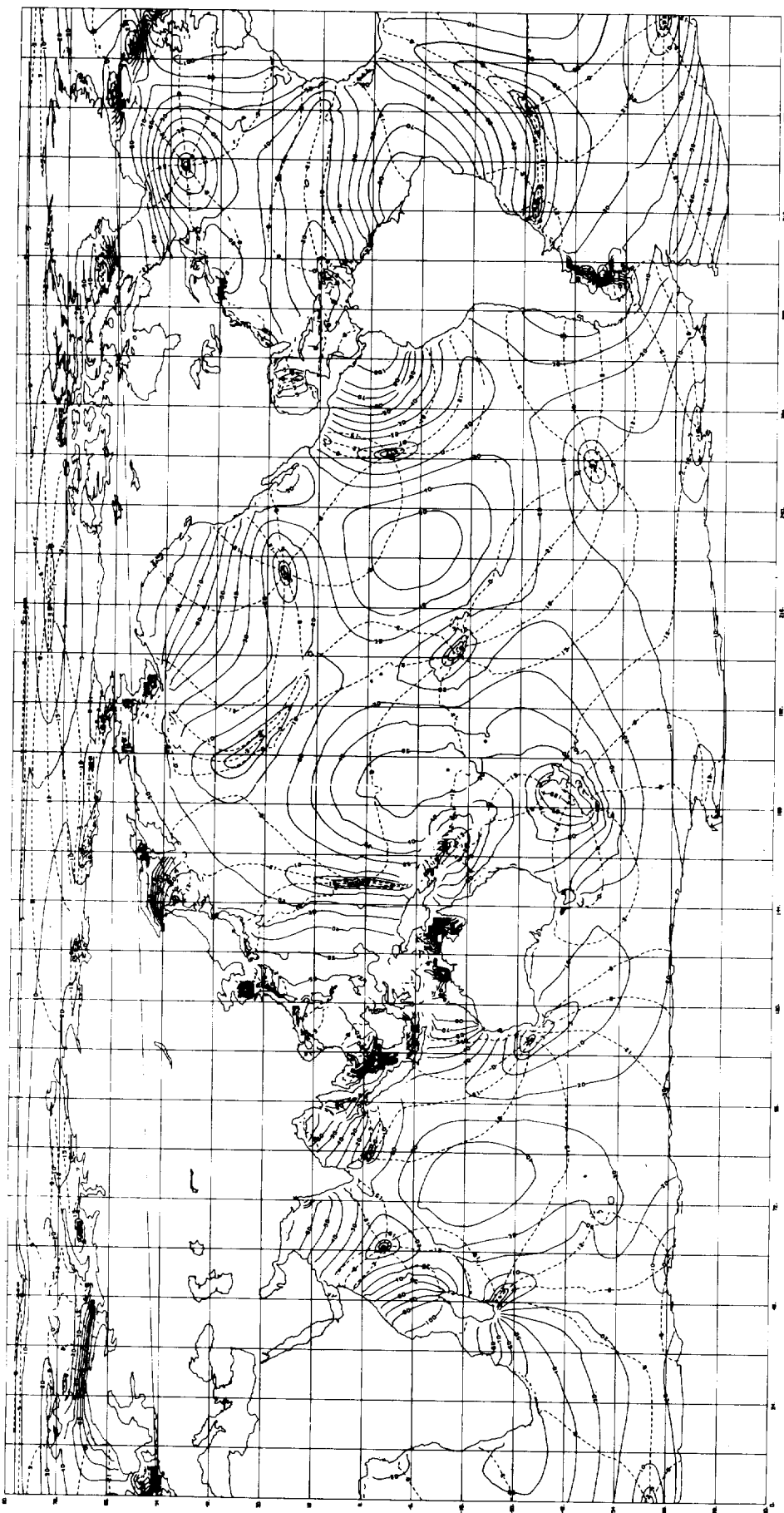


Fig. 8. Schwiderski global M_2 tide model (plot courtesy of R. H. Estes). Solid contours are amplitudes ξ in centimeters. Dashed contours are phases δ in $\frac{1}{4}$ lunar hours.

1979b,
Figure
(12)) of
Natural
near co-
and near
tide and
dictions
tuaries,
sufficient
known
fant, 19
high-ac-

b. Cor-

Begin
tific cha-
votion o
and the
myths, a
rich and
up to the
ings of
Geodesy,
Ocean L
global o
which sa
at least i

The r
computa
 P_1 , Q_1),
the sam
of these
Zahel [1
 O_1 , P_1),
cad and
 b , c ,] ha
ponents
are curr
Estes th
(section
due to t
that the
empirical
the some
be attribu
tides to

While
by coor
made by
fields, t
techniques
tide data
significa
limited a
tide data
The ben
the rema
achieved
sult is e
duced by
cal wave
[Kuo et

1979b, c] estimated that his model (schematically shown in Figure 8) permits a tide prediction with an error (equation (12)) of generally less than 5 cm anywhere in the open ocean. Naturally, the achieved high accuracy may drop off somewhat near continental and island stations (e.g., in the Arctic Sea and near Antarctica) where only sporadic or erratic empirical tide and bathymetric data are known. Also, less accurate predictions must be anticipated in small border seas, bays, estuaries, and channels, where the $1^\circ \times 1^\circ$ network precludes a sufficient resolution. For example, Table 4b displays the well-known amphidromic point in the Gulf of Saint Lawrence [Defant, 1961], but the mesh size is much too coarse to permit a high-accuracy pointwise resolution.

b. Conclusions

Beginning with Newton, through three centuries the scientific charting of tides in the world oceans has captured the devotion of many scientists and mathematicians. Experimental and theoretical progress advance slowly through paradoxes, myths, and controversies. In the preceding review sections this rich and fascinating work has been highlighted and analyzed up to the present state of the art. In agreement with the findings of the *International Workshop on Interaction of Marine Geodesy with Inertial, Tidal, and High Frequency Aspects of Ocean Dynamics* [1978] in Miami it is concluded that the total global ocean tide can now be computed with an accuracy which satisfies the 10-cm error bound set by modern tide users at least in open ocean regions.

The missing final step requires essentially only the actual computation of the 10 tidal components (S_2, N_2, K_2), (K_1, O_1, P_1, Q_1), and (M_f, M_m, Ssa) which must be constructed with the same accuracy as the M_2 tide. Recent tidal maps of some of these constituents have been computed, for example, by Zahel [1973, 1977] for K_1 ; Estes [1977] for (S_2, N_2, K_2) and (K_1, O_1, P_1); Parke and Hendershott [1979] for S_2 and K_1 , and Accad and Pekeris [1978] for S_2 . The author [Schwiderski, 1980a, b, c.] has completed his own computations of the leading components S_2 and (K_1, O_1). The remaining minor partial tides are currently being processed. In agreement with Zahel and Estes the author detected no resonance or stability problems (section 2c) for any of the computed tides, which is obviously due to the modeled dissipation forces. It may be mentioned that the author noticed a distinctly tapered roughness in the empirical and computed data of the diurnal tides relative to the sometimes tumbling semidiurnal tides. This probably can be attributed to the doubled periods, which allow the diurnal tides to assume a calmer level.

While the successful charting of ocean tides was achieved by coordinating the various contributions and experiences made by numerous researchers in oceanography and related fields, the most dramatic improvement of the modeling techniques can be attributed to the direct inclusion of empirical tide data. As was observed by the author, in contrast to other significant improvements, which were often effective only in limited areas, the hydrodynamic interpolation of empirical tide data produced a correction uniformly over all oceans. The beneficial effects of empirical data are also apparent from the remarkable quality which Parke and Hendershott [1979] achieved with a rather coarse grid system. This important result is even more borne out by the limited-area maps produced by ordinary interpolation of empirical data using classical wave elements [Munk et al., 1970], low-degree polynomials [Kuo et al. 1970a, b], or simple rules of thumb [Dietrich,

1944a, b; Bogdanov, 1961a, b; Luther and Wunsch, 1975]. Ironically, the latter maps based on pure intuition and experience reflect a higher quality than some computed charts.

Though the charting of worldwide ocean tides has reached a first level of satisfactory numerical accuracy, the tidal phenomenon remains as alluring as ever. Future precise measurements of ocean tides and the search for their accurate harmonic analyses must be encouraged in order to check and, where it is necessary, improve the established models. In particular, improvements can be expected from new empirical data where present tide or bathymetric values are marginal, rough, or unreliable. In irregular ocean regions, for instance, in front of large rivers and coastal corners, the global tide models should be supplemented by limited-area models. Such models may include refined grid systems with more realistic dissipation forces. In fact, nearshore models of this kind are of immediate interest in many applications. New promising approaches to utilizing modern satellite technology for the experimental determination of open ocean tides have been reported by Estes [1979] and J. M. Diamante (private communication, 1978).

Acknowledgments. It is the author's most pleasant obligation to thank the Editor, J. W. Chamberlain, and the Associated Editor, F. Morrison, of *Reviews of Geophysics and Space Physics* for their invitation and patient encouragement to prepare this comprehensive review article. This project was supported by the Naval Surface Weapons Center (NAVSWC) Independent Research Fund and by a grant from the National Geodetic Survey/NOS/NOAA. Special acknowledgment is extended to Ralph A. Niemann, head of the Strategic Systems Department, R. J. Anderle, head of the Astronautics and Geodesy Division, and his associate, C. Oesterwinter, for their sustained and generous sponsorship of the author's entire work on ocean tidal modeling that included seemingly unending computer experiments. The involved computer programs were all prepared by L. Szeto in a competent and effective manner. Many critical and stimulating suggestions were gratefully received from the author's NAVSWC colleagues C. J. Cohen and B. Zondek. The author wishes to thank R. H. Estes of Business and Technological Systems, Inc., for his courtesy in undertaking the difficult task of mapping (Figure 8) the author's tide model. Also, R. H. Estes communicated to the author copies of the prepublication papers by Parke [1978] and Accad and Pekeris [1978]. Other helpful papers, empirical data, and suggestions were received with gratitude from D. E. Cartwright, Institute of Oceanographic Sciences, Birkenhead, United Kingdom; S. K. Gill, NOS/NOAA; B. Kagan, Institute of Oceanography, Leningrad, USSR; J. T. Kuo and F. Malone, Lamont-Doherty Geological Observatory, Columbia University; H. O. Mofjeld, Pacific Marine Environmental Laboratory (PMEL/NOAA); W. H. Munk, Scripps Institution of Oceanography (SIO); M. E. Parke, Jet Propulsion Laboratory; C. A. Pearson, PMEL/NOAA; W. J. Pierson, Jr., Cuny Institute of Marine and Atmospheric Sciences, New York City College; D. L. Porter, NOS/NOAA; M. Schulkin, Applied Physics Laboratory, University of Washington; D. C. Simpson, NOS/NOAA; K. Wyrtki, University of Hawaii; B. D. Zetler, SIO; the International Hydrographic Bureau, Monaco; the Hydrographer of the Navy, United Kingdom; the Marine Environmental Data Service, Canada; and the Rand Corporation, Santa Monica, California.

REFERENCES

- Accad, Y., and C. L. Pekeris, The K_2 tide in oceans bounded by meridians and parallels, *Proc. Roy. Soc. London, Ser. A*, 278, 110, 1963.
- Accad, Y., and C. L. Pekeris, Solution of the tidal equations for M_2 and S_2 tides in the world oceans from a knowledge of the tidal potential alone, *Phil. Trans. Roy. Soc. London, Ser. A*, 290, 235, 1978.
- Airy, G. B., Tides and waves, *Encyclo. Metrop. London*, 5, 241, 1842.
- Bartels, J., Gezeitenkräfte, *Handb. Phys.*, XLVIII, *Geophys. II*, 1957.
- Berghaus, H., *Physikalischer Handatlas*, Gotha, East Germany, 1845.
- Bogdanov, C. T., New charts of the cotidal lines of semidiurnal tide waves (M_2 and S_2) for the Pacific Ocean, *Sov. Oceanogr., Engl. Transl.*, I, 28, 1961a.

- Bogdanov, C. T., New charts of the diurnal tide (K_1 and O_1) for the Pacific Ocean, *Sov. Oceanogr. Engl. Transl.*, I, 46, 1961b.
- Bogdanov, C. T., and V. A. Magarik, A numerical solution of the problem of semidiurnal tidal wave distribution (M_2 and S_2) in the ocean, (in Russian), *Dokl. Akad. Nauk SSSR*, 172, 1315, 1967.
- Bogdanov, C. T., and V. A. Magarik, A numerical solution of the problem of tidal wave propagation in the world ocean (in Russian), *Izv. Akad. Nauk SSSR Fiz. Atmos. Okeana*, 5, 1309, 1969.
- Bogdanov, C. T., K. V. Kim, and V. A. Magarik, A numerical solution of the hydrodynamical equations of tides on the BESM-2 computer for the world ocean area (in Russia), *Tr. Inst. Okeanol. Akad. Nauk SSSR*, 75, 73, 1964.
- Boussinesq, J., Théorie de l'écoulement tourbillant, *Mem. Presentes Acad. Sci.*, XXIII, 46, 360, 1877.
- Boussinesq, J., Expression du frottement extérieur dans l'écoulement tumultueux d'une fluide, *C. R. Acad. Sci.*, 122, 1445, 1896.
- Bretschneider, G., Anwendung des hydrodynamisch-numerischen Verfahrens zur Ermittlung der M_2 -mittschwingungszeit der Nordsee, *Mitt. Inst. Meereskunde Univ. Hamburg*, VII, 1967.
- British Admiralty, *Tide Tables*, vols. 1-3, Hydrographer of the Navy, London, 1977.
- Bryan, K., A numerical investigation of a nonlinear model of a wind-driven ocean, *J. Atmos. Sci.*, 20, 594, 1963.
- Busse, F. H., and J. A. Whitehead, Instabilities of convection rolls in a high Prandtl number fluid, *J. Fluid Mech.*, 47, 305, 1971.
- Cantor, G., *Vorlesungen Über Geschichte der Mathematik*, vol. 3, W. de Gruyter, Leipzig, East Germany, 1901.
- Cartwright, D. E., A unified analysis of tides and surges around north and east Britain, *Phil. Trans. Roy. Soc. London*, Ser. A, 263, 1, 1968.
- Cartwright, D. E., Extraordinary tidal currents near St. Kilda, *Nature*, 223, 938, 1969.
- Cartwright, D. E., Tides and waves in the vicinity of St. Helena, *Phil. Trans. Roy. Soc. London*, Ser. A, 270, 603, 1971.
- Cartwright, D. E., Oceanic tides, *Rep. Progr. Phys.*, 40, 665, 1977.
- Cartwright, D. E., B. D. Zetler, and B. V. Hamon, *Pelagic Tidal Constants*, Publ. Sci. 30, International Association of Physical Sciences of the Oceans, 1979.
- Cartwright, D. E., and R. J. Tayler, New computations of the tide-generating potential, *Geophys. J. Roy. Astron. Soc.*, 23, 45, 1971.
- Cartwright, D. E., W. H. Munk, and B. D. Zetler, Pelagic tidal measurements, *Eos Trans. AGU*, 50, 472, 1969.
- Cox, M. D., A mathematical model of the Indian Ocean, *Deep Sea Res.*, 17, 45, 1970.
- Crowley, W. P., A global numerical model, I, *J. Comput. Phys.*, 3, 111, 1968.
- Crowley, W. P., A numerical model for viscous, free-surface barotropic wind-driven ocean circulations, *J. Comput. Phys.*, 5, 139, 1970.
- Darwin, G. H., Report on the harmonic analysis of tidal observations, Brit. Ass. for the Advan. of Sci., London, 1883.
- Defant, A., Flutwellen und Gezeiten des Wassers, *Handb. Phys.*, XLVIII, *Geophys.* II, 846, 1957.
- Defant, A., *Physical Oceanography*, vol. II, Pergamon, New York, 1961.
- Dietrich, G., Die Gezeiten des Weltmeeres als geographische Erscheinung, *Z. Gesamte Erdk.*, 3, 69, 1944a.
- Dietrich, G., Die Schwingungssysteme der halb-und eintägigen Tiden in den Ozeanen, *Veroeff. Inst. Meereskunde Univ. Berlin*, 41, 1944b.
- Dietrich, G., *General Oceanography*, Wiley-Interscience, New York, 1963.
- Dishon, M., Determination of the average ocean depths from bathymetric data, *Int. Hydrogr. Rev.*, 41, 77, 1964.
- Dishon, M., and B. C. Heezen, Digital deep-sea sounding library, *Int. Hydrogr. Rev.*, 45, 23, 1968.
- Doodson, A. T., The harmonic development of the tide-generating potential, *Proc. Roy. Soc. London*, Ser. A, 100, 305, 1921.
- Döös, B. R., et al., Modeling for the first Garp global experiment, *Garp Publ. Ser. 14*, Int. Counc. of Sci. Unions, Paris, 1974.
- Ekman, V. W., Om jordrotationens inverkan på vindströmmar i havet, *Nyt Mag. Naturvidensk.*, 20, 67, 1902.
- Estes, R., A computer software system for the generation of global numerical solutions of diurnal and semidiurnal ocean tides, *Rep. TR-75-27*, Bus. and Technol. Syst., Greenbelt, Md., 1975.
- Estes, R., A computer software system for the generation of global ocean tides and crustal loading effects, *Rep. TR-77-41*, Bus. and Technol. Syst., Greenbelt, Md., 1977.
- Estes, R., A simulation of global ocean tide recovery using altimeter data with systematic orbit error, *J. Mar. Geod.*, in press, 1979.
- Eyries, M., Maregraphs de grandes profondeurs, *Cah. Oceanogr.*, 20, 335, 1968.
- Farrell, W. E., Deformation of the earth by surface loads, *Rev. Geophys. Space Phys.*, 10, 261, 1972a.
- Farrell, W. E., Global calculations of tidal loading, *Nature*, 238, 43, 1972b.
- Farrell, W. E., Earth tides, ocean tides, and tidal loading, *Phil. Trans. Roy. Soc. London*, Ser. A, 274, 253, 1973.
- Ferrel, W., Tidal researches, report, pp. 154, 239, 245, U.S. Coast and Geod. Surv., Washington, D. C., 1874.
- Filloux, J. H., Bourbon tube deep-sea tide gages, in *Proceedings of the Symposium on Tsunamis and Tsunami Research*, Honolulu, Int. Union of Geod. and Geophys., Paris, 1969.
- Fomin, L. M., *The Dynamic Method in Oceanography*, Elsevier, New York, 1964.
- Friedrich, H. J., Numerische Berechnung der allgemeinen Zirkulation im Meer nach einem Differenzen Verfahren, Vornehmlich für den Atlantischen Ozean, *Mitt. Inst. Meereskunde Univ. Hamburg*, III, 1966.
- Friedrich, H. J., Preliminary results from a numerical multilayer model for the circulation in the North Atlantic, *Deut. Hydrogr. Z.*, 23, 145, 1970.
- Gallagher, B. S., K. M. Shimada, F. L. Gonzales, Jr., and E. D. Stroup, Tides and currents in Fanning atoll lagoon, *Pac. Sci.*, 25, 191, 1971.
- Gates, L. R., and A. B. Nelson, A new (revised) tabulation of the Scripps topography on a 1° global grid, II, Ocean depths, *Rep. 1277*, Rand Corp., Santa Monica, Calif., 1975.
- Gill, S. K., and D. L. Porter, Comparison of results from a simple De-fant tidal model with observed offshore tides, *J. Mar. Geod.*, in press, 1979.
- Goad, C. C., and B. C. Douglas, Determination of the M_2 ocean tide parameters from satellite orbit perturbations, *J. Geophys. Res.*, 82, 88, 1977a.
- Goad, C. C., and B. C. Douglas, Lunar longitude deceleration and tidal parameters estimated from satellite orbital perturbations, paper presented at the Eighth International Symposium on Earth Tides, Bonn, Federal Republic of Germany, Int. Ass. of Phys. Sci. of the Oceans, 1977b.
- Gohin, F., Determination des denivellations et des courants de marée, *Proc. Conf. Coastal Eng.* 7th, 2, 485, 1961.
- Gordeyev, R. G., B. A. Kagan, and V. Y. Rivkind, Numerical solution of the dynamic tidal equations in the global ocean (in Russian), *Dokl. Akad. Nauk SSSR*, 209, 340, 1973.
- Gordeyev, R. G., B. A. Kagan, and E. Polyakov, The effects of loading and self attraction on global ocean tides, the model and the results of a numerical experiment, *J. Phys. Oceanogr.*, 7, 161, 1977.
- Grace, S. F., The semidiurnal tidal motion of the Red Sea, *Mon. Notic. Roy. Astron. Soc., Geophys. Suppl.*, 2, 274, 1930a.
- Grace, S. F., The influence of the friction on the tidal motion of the Gulf of Suez, *Mon. Notic. Roy. Astron. Soc., Geophys. Suppl.*, 2, 316, 1930b.
- Hansen, W., Die Ermittlung der Gezeiten Beliebig Gestalteter Meeresgebiete mit Hilfe des Randwertverfahrens, *Deut. Hydrogr. Z.*, 1, 157, 1948.
- Hansen, W., Die halbtägigen Gezeiten im Nordatlantischen Ozean, *Deut. Hydrogr. Z.*, 2, 44, 1949.
- Hansen, W., Die Reproduktion der Bewegungsvorgänge im Meere mit Hilfe hydrodynamisch-numerischer Verfahren, *Mitt. Inst. Meereskunde Univ. Hamburg*, V, 1966.
- Harris, R. A., Manual of tides, IVb, Report of the Superintendent, p. 313, U.S. Coast and Geod. Surv., Washington, D. C., 1904.
- Hendershott, M. C., The effects of solid-earth deformation on global ocean tides, *Geophys. J. Roy. Astron. Soc.*, 29, 380, 1972.
- Hendershott, M. C., Ocean tides, *Eos Trans. AGU*, 54, 76, 1973.
- Hendershott, M. C., Global numerical tide solutions with inclusion of ocean self-gravitation and of solid earth tidal loading, paper presented at XVI General Assembly, Int. Union of Geod. and Geophys., Grenoble, France, 1975.
- Hendershott, M. C., Numerical models of ocean tides, in *The Sea*, vol. 6, p. 47, John Wiley, New York, 1977.
- Hendershott, M. C., and W. H. Munk, Tides, *Annu. Rev. Fluid Mech.*, 2, 205, 1970.
- Holland, W. R., and A. D. Hirschman, A numerical calculation of the

- circulation in the North Atlantic Ocean, *J. Phys. Oceanogr.*, 2, 336, 1972.
- Hopfner, F., 1931. Die Gezeiten der Meere, in *Handbuch der Experimentalphysik, Geophysik*, vol. 2, Akademische, Leipzig, East Germany, 1931.
- Hough, S., On the application of harmonic analysis to the dynamical theory of the tides, *Phil. Trans. Roy. Soc. London, Ser. A*, 219, 201, 1897.
- International Hydrographic Bureau, Tides, harmonic constants, *Spec. Publ.* 26, Monaco, 1966.
- International Workshop on Interaction of Marine Geodesy With Inertial, Tidal, and High Frequency Aspects of Ocean Dynamics, report presented at the International Symposium on Interaction of Marine Geodesy and Ocean Dynamics, Miami, 1978.
- International Working Group on Ocean Tides, report presented at the XVI General Assembly, Int. Union of Geod. and Geophys., Grenoble, France, 1975.
- Irish, J. D., and F. E. Snodgrass, Australian-Antarctic tides, in *Antarctic Oceanology, II, The Australian-New Zealand Sector, Antarctica Res. Ser.*, vol. 19, edited by D. E. Hayes, p. 101, AGU, Washington, D. C., 1972.
- Irish, J. D., W. H. Munk, and F. E. Snodgrass, M_2 amphidrome in the northeast Pacific, *Geophys. Fluid Dyn.*, 2, 355, 1971.
- Jachens, R. C., and J. T. Kuo, The O_1 tide in the North Atlantic Ocean as derived from land-based tidal gravity measurements, in *Proceedings of the Seventh Symposium on Earth Tides, Sopron, Hungary*, Akad. Kiado, Budapest, 1973.
- Johns, B., Vertical structure of tidal flows in river estuaries, *Geophys. J. Roy. Astron. Soc.*, 12, 103, 1966.
- Kagan, B. A., Bottom friction in a one-dimensional tidal flow, *Izv. Acad. Sci. USSR Atmos. Oceanic Phys.*, Engl. Transl., 7, no. 11, 1971.
- Kagan, B. A., Resistance law of tidal flow, *Izv. Acad. Sci. USSR Atmos. Oceanic Phys.*, Engl. Transl., 8, no. 5, 1972.
- Kagan, B. A., Global interaction of ocean and terrestrial tides (in Russian), in *News and Problems of Science Gidrometeoizdat*, Leningrad, 1977.
- Kuo, J. T., R. C. Jachens, G. White, and M. Ewing, Tidal gravity measurements along a transcontinental profile across the United States, *Comm. Observ. Roy. Belg.*, no. 9, 96, 1970a.
- Kuo, J. T., R. C. Jachens, M. Ewing, and G. White, Transcontinental tidal gravity profile across the United States, *Science*, 168, 968, 1970b.
- Kuo, J. T., R. C. Jachens, and S. S. Lee, The northeastern Pacific O_1 and the North Atlantic M_2 ocean tides as derived from inversion, paper presented at the Eighth International Symposium on Earth Tides, Bonn, Federal Republic of Germany, Int. Ass. of Phys. Sci. of the Oceans, 1977.
- Ladyzhenskaya, O. A., *The Mathematical Theory of Viscous Incompressible Flow*, Gordon and Breach, New York, 1969.
- Lamb, H., *Hydrodynamics*, Dover, New York, 1932.
- Lamb, H., and L. Swain, A tidal problem, *Phil. Mag.*, 29, 737, 1915.
- Laplace, P. S., Recherches sur quelques points de système du monde, *Mem. Acad. Roy. Soc.*, 88, 177, 1775.
- Larsen, L. H., and J. D. Irish, Tides at Cobb Seamount, *J. Geophys. Res.*, 80, 1691, 1975.
- Leith, C. E., Two-dimensional eddy viscosity coefficients, in *Proceedings of the WMO/IUGG Symposium on Numerical Weather Prediction, Tokyo*, p. 140, World Meteorological Organization, Geneva, 1968.
- Luther, D. S., and C. Wunsch, Tidal charts of the central Pacific Ocean, *J. Phys. Oceanogr.*, 5, 227, 1975.
- Marchuk, G. I., and B. A. Kagan, *Ocean Tides: Mathematical Models of Numerical Experiments* (in Russian), Gidrometeoizdat, Leningrad, 1977.
- Marchuk, G. I., B. A. Kagan, and R. E. Tamsalu, A numerical method of calculating tidal motion in border seas, *Izv. Acad. Sci. USSR Atmos. Oceanic Phys.*, Engl. Transl., 5, 694, 1969.
- Marchuk, G. I., R. G. Gordeyev, V. Y. Rivkind, and B. A. Kagan, A numerical method for the solution of tidal dynamics equations and the results of its application, *J. Comput. Phys.*, 13, 15, 1973.
- McGregor, R. C., The influence of eddy viscosity on the vertical distribution of velocity in the tidal estuary, *Geophys. J. Roy. Astron. Soc.*, 29, 103, 1972.
- Miles, J., On Laplace's tidal equations, *J. Fluid Mech.*, 66, 241, 1974.
- Miyazaki, M., S. Kuronuma, and T. Inoue, Tidal constants along the coast of Japan, *Oceanogr. Mag.*, 19, 13, 1967.
- Mofjeld, H. O., Empirical model for tides in the western North Atlantic Ocean, *Rep. TR ERL 340-AOML19*, Nat. Oceanic and Atmos. Admin., Boulder, Colo., 1975.
- Munk, W. H., On the wind-driven ocean circulation, in *Wind-Driven Ocean Circulation*, Blaisdell, New York, 1963.
- Munk, W. H., Abyssal recipes, *Deep Sea Res.*, 13, 707, 1966.
- Munk, W. H., and D. E. Cartwright, Tidal spectroscopy and prediction, *Phil. Trans. Roy. Soc. London, Ser. A*, 259, 533, 1966.
- Munk, W. H., and E. Palmén, Note on the dynamics of the antarctic circumpolar current, *Tellus*, 3, 53, 1951.
- Munk, W. H., F. Snodgrass, and M. Wimbush, Tides offshore: Transition from California coastal to deep-sea waters, *Geophys. Fluid Dyn.*, 1, 161, 1970.
- National Ocean Survey, Tidal harmonic constants, report, U.S. Coast and Geod. Surv., Washington, D. C., 1942.
- Neumann, G., and W. J. Pierson, Jr., *Principles of Physical Oceanography*, Prentice-Hall, Englewood Cliffs, N. J., 1966.
- Newton, I., *Philosophiae Naturalis Principia Mathematica*, London, 1687. (Also in *Oceanography Concepts and History*, edited by M. B. Deacon, Dowden, Hutchinson, and Ross, Stroudsburg, Pa., 1978.)
- Nowroozi, A. A., Long-term measurements of pelagic tidal height off the coast of northern California, *J. Geophys. Res.*, 77, 434, 1972.
- Noye, J., and A. K. Easton, The computation of tidal constants, *Comput. Programmes 7*, Horace Lamb Centre, Flinders Univ. of S. Australia, 1967.
- O'Brien, J. J., A two-dimensional model of the wind-driven North Pacific Invest. *Pesq.*, 35, 331, 1971.
- Parke, M. E., Open ocean tide modelling, paper presented at the 9th Geodesy, Solid Earth, and Ocean Physics Research Conference, Int. Union of Geod. and Geophys., Columbus, Ohio, Oct. 1978.
- Parke, M. E., and M. C. Hendershot, M_2 , S_2 , and K_1 models of the global ocean tide on an elastic earth, *J. Mar. Geod.*, in press, 1979.
- Pearson, C. A., Deep-sea tide and current observations in the Gulf of Alaska and northeast Pacific, *Tech. Memo. NOS 16*, Nat. Oceanic and Atmos. Admin., Rockville, Md., 1975a.
- Pearson, C. A., Deep-sea tide observations off the southeastern United States, *Tech. Memo. NOS 17*, Nat. Oceanic and Atmos. Admin., Rockville, Md., 1975b.
- Pekeris, C. L., and Y. Accad, Solution of Laplace's equation for the M_2 tide in the world oceans, *Phil. Trans. Roy. Soc. London, Ser. A*, 265, 413, 1969.
- Platzman, G. W., *Ocean Tides and Related Waves, Lect. Appl. Math.*, vol. 14, American Mathematical Society, Providence, R. I., 1971.
- Platzman, G. W., Two-dimensional free oscillations in natural basins, *J. Phys. Oceanogr.*, 2, 117, 1972a.
- Platzman, G. W., North Atlantic Ocean: Preliminary description of normal modes, *Science*, 178, 156, 1972b.
- Platzman, G. W., Normal modes of the Atlantic and Indian oceans, *J. Phys. Oceanogr.*, 5, 201, 1975.
- Poincaré, H., *Leçons de Mécanique Céleste*, vol. 3, *Theorie des Marées*, Gauthier-Villars, Paris, 1910.
- Prandtl, L., Über die ausgebildete Turbulenz, *Z. Angew. Math. Mech.*, 5, 136, 1925.
- Proudman, J., Free and forced longitudinal tidal motion in a lake, *Proc. London Math. Soc.*, 14, 2, 1915.
- Proudman, J., *Dynamical Oceanography*, Dover, New York, 1952.
- Proudman, J., and A. T. Doodson, On the tides in an ocean bounded by two meridians on a nonrotating earth, *Mon. Notic. Roy. Astron. Soc., Geophys. Suppl.*, 1, 468, 1927.
- Reid, R. O., A. R. Robinson, and K. Bryan, *Numerical Models of Ocean Circulation*, National Academy of Sciences, Washington, D. C., 1975.
- Richardson, L. F., *Weather Prediction by Numerical Methods*, Cambridge University Press, New York, 1922.
- Richtmyer, R. D., and K. W. Morton, *Difference Methods for Initial Value Problems*, Interscience, New York, 1967.
- Schlichting, H., *Boundary-Layer Theory*, McGraw-Hill, New York, 1968.
- Schwiderski, E. W., Bifurcation of convection in internally heated fluid layers, *Phys. Fluids*, 15, 1882, 1972.
- Schwiderski, E. W., Preliminary M_2 tide, computer tape, Nav. Surface Weapons Center, Dahlgren, Va., 1976.
- Schwiderski, E. W., Hydrodynamically defined ocean bathymetry,

- Rep. NSWC/DL TR 3888*, Nav. Surface Weapons Center, Dahlgren, Va., 1978a.
- Schwiderski, E. W., Global ocean tides, I, A detailed hydrodynamical interpolation model, *Rep. NSWC/DL TR 3866*, Nav. Surface Weapons Center, Dahlgren, Va., 1978b.
- Schwiderski, E. W., Ocean tides, I, Global ocean tidal equations, *J. Mar. Geod.*, in press, 1979a.
- Schwiderski, E. W., Ocean tides, II, A hydrodynamical interpolation model, *J. Mar. Geod.*, in press, 1979b.
- Schwiderski, E. W., Global ocean tides, II, The semidiurnal principal lunar tide (M_2), report, Nav. Surface Weapons Center, Dahlgren, Va., in press, 1979c.
- Schwiderski, E. W., Global ocean tides, III, The semidiurnal principal solar tide (S_2), report, Nav. Surface Weapons Center, Dahlgren, Va., in press, 1980a.
- Schwiderski, E. W., Global ocean tides, IV, The diurnal luni-solar declination tide (K_1), report, Nav. Surface Weapons Center, Dahlgren, Va., in press, 1980b.
- Schwiderski, E. W., Global ocean tides, V, The diurnal principal lunar tide (O_1), report, Nav. Surface Weapons Center, Dahlgren, Va., in press, 1980c.
- Shilov, G. E., *Generalized Functions and Partial Differential Equations*, Gordon and Breach, New York, 1968.
- Smagorinsky, J., General circulation experiments with the primitive equations, I, The basic experiment, *Mon. Weather Rev.*, 91, 99, 1963.
- Smith, S. M., H. M. Menard, and G. Sharman, Worldwide ocean depths and continental elevations averaged for areas approximating one-degree squares of latitude and longitude, *Ref. 65-8*, Scripps Inst. of Oceanogr., La Jolla, Calif., 1966.
- Snodgrass, F. E., Deep-sea instrument capsule, *Science*, 162, 78, 1968.
- Stern, M. E., *Ocean Circulation Physics*, Academic, New York, 1975.
- Sterneck, R. V., Die Gezeiten der Ozeane, 1, *Mitt. Sitzungsberg. Akad. Wiss. Wien*, 129, 131, 1920.
- Sterneck, R. V., Die Gezeiten der Ozeane, 2, *Mitt. Sitzungsber. Akad. Wiss. Wien*, 130, 363, 1921.
- Stommel, H., *The Gulf Stream*, University of California Press, Berkeley, 1960.
- Taylor, G. I., Tidal friction in the Irish Sea, *Phil. Trans. Roy. Soc., Ser. A*, 220, 1, 1918.
- Thomson, W. (Lord Kelvin), Report of committee for the purpose of harmonic analysis of tidal observations, Brit. Ass. for the Advan. of Sci., London, 1868.
- Thomson, W. (Lord Kelvin), On gravitational oscillations of rotating water, *Proc. Roy. Soc. Edinburgh*, 10, 141, 1879.
- Tiron, K. D., Y. N. Sergeev, and A. N. Michurin, Tidal charts for the Pacific, Atlantic, and Indian oceans, *Vestn. Leningrad. Univ., Engl. Transl.*, 24, 122, 1967.
- Trepka, L. V., Anwendung des hydrodynamisch-numerischen Verfahrens zur Ermittlung des Schelfeinflusses auf die Gezeiten in Modellkanälen und Modellozeanen, *Mitt. Inst. Meereskunde Univ. Hamburg*, IX, 1967.
- Ueno, T., Theoretical studies on tidal waves traveling over the rotating globe, I, *Oceanogr. Mag.*, 15, 99, 1964a.
- Ueno, T., Theoretical studies on tidal waves traveling over the rotating globe, II, *Oceanogr. Mag.*, 16, 47, 1964b.
- Villain, C., Cartes des lignes cotidales dans les Océans, *Ann. Hydrog. Paris*, 3, 269, 1952.
- Whewell, W., Essay towards a first approximation to a map of cotidal lines, *Phil. Trans. Roy. Soc. London*, I, 147, 1833.
- Whewell, W., On the tides of the Pacific and on the diurnal inequality, *Phil. Trans. Roy. Soc. London*, 16, I, 1848.
- Whitaker, S., *Introduction to Fluid Mechanics*, Prentice-Hall, Englewood Cliffs, N. J., 1968.
- Zahel, W., Die Reproduktion gezeitenbedingter Bewegungsvorgänge im Weltmeer Mittels des hydrodynamisch-numerischen Verfahrens, *Mitt. Inst. Meereskunde Univ. Hamburg*, XVII, 1970.
- Zahel, W., The diurnal K_1 tide in the world ocean—A numerical investigation, *Pure Appl. Geophys.*, 109, 1819, 1973.
- Zahel, W., A global hydrodynamic-numerical 1° -model of the ocean tides: The oscillation system of the M_2 -tide and its distribution of energy dissipation, paper presented at XVI General Assembly, Int. Union Geod. Geophys., Grenoble, France, 1975.
- Zahel, W., The influence of solid earth deformations on semidiurnal and diurnal oceanic tides, in *Tidal Friction and Earth's Rotation*, edited by P. Brosche and J. Sündermann, p. 98, Springer, New York, 1977.
- Zetler, B., W. Munk, H. Mofjeld, W. Brown, and F. Dorner, Mode tides, *J. Phys. Oceanogr.*, 5, 430, 1975.

(Received February 22, 1979;
accepted July 19, 1979.)

Introdu
Heat fl
Intro
Data
Ther
Hyd
Rein
Mar
Man
Conti
Intr
Geo
Con
Heat
Heat
The
Heat l
Intr
Heat
Heat
Tot
This
the A
Paper